NOVEL CONCRETE CHEMISTRY ACHIEVED WITH LOW DOSE GAMMA RADIATION CURING AND RESISTANCE TO NEUTRON ACTIVATION

by

Steven Robert Burnham

A dissertation submitted to the faculty of
The University of Utah
in partial fulfillment of the requirements for the degree of

Doctor of Philosophy

in

Nuclear Engineering

Department of Civil and Environmental Engineering

The University of Utah

May 2017

The University of Utah Graduate School

STATEMENT OF DISSERTATION APPROVAL

The dissertation of **Steven Robert Burnham**

has been approved by the following supervisory committee members:

Tatjana Jevremovic	, Chair	**2/24/2017** Date Approved
Masoud Beitollahi	, Member	**2/24/2017** Date Approved
Sivaraman Guruswamy	, Member	**2/24/2017** Date Approved
Swomitra Mohanty	, Member	**2/24/2017** Date Approved
Terry Ring	, Member	**2/24/2017** Date Approved

and by **Michael Barber**, Chair/Dean of

the Department/College/School of **Civil and Environmental Engineering**

and by David B. Kieda, Dean of The Graduate School.

ABSTRACT

As much as 50% of ageing-related problems with concrete structures can be attributed to construction deficiencies at the time of placement. The most influential time affecting longevity of concrete structures is the curing phase, or commonly the initial 28 days following its placement. A novel advanced atomistic analysis of novel concrete chemistry is presented in this dissertation with the objective to improve concrete structural properties and its longevity. Based on experiments and computational models, this novel concrete chemistry is discussed in two cases: (a) concrete chemistry changes when exposed to low-dose gamma radiation in its early curing stage, thus improving its strength in a shorter period of time then curing for the conventional 28 days; (b) concrete chemistry is controlled by its atomistic components to assure strength is not reduced but that its activation due to long-term exposure to neutron flux in nuclear power plants is negligible. High dose gamma radiation is well documented as a degradation mechanism that decreases concrete's compressive strength; however, the effects of low-dose gamma radiation on the initial curing phase of concrete, having never been studied before, proved its compressive strength increases. Using a ^{137}Cs source, concrete samples were subjected to gamma radiation during the initial curing phase for seven, 14, and 28 days. The compressive strength after seven days is improved for gamma cured concrete by 24% and after 14 days by 76%. Concrete shows no improvement in compressive strength after 28 days of exposure to gamma radiation, showing that there is a threshold effect. Scanning Electron Microscopy is used to examine the microstructure of low-dose gamma radiation where no damage to its microstructure is found, showing no difference between gamma cured and conventionally cured concrete. Molecular dynamics modeling based on the MOPAC package is used to study how gamma radiation during the curing stage improves compressive strength of concrete. The modeling shows that when radiolysis occurs in freshly mixed concrete, the reactivity between key molecules responsible for bonding between cement and aggregate is enhanced due to improved reactivity at the molecular level. A new method is developed that successfully controls a concrete chemistry at the atomistic level by assuring its long-term exposure to neutron flux in nuclear power plants will not activate the dome wall to the level of low-level radioactive waste. This methodology is established to detect and select the level of trace elemental composition in concrete based on a low-flux neutron activation analysis (NAA). By carefully selecting aggregates that do not contain certain elements

that activate to high concentrations after decades of concrete exposure to neutron flux, the end of life for concrete is improved by declassifying it as low-level radioactive waste. Directly, it improves economy of commissioning nuclear power plants to be built in near future and reducing important quantities of waste to be disposed at high costs.

CONTENTS

LIST OF TABLES

ACKNOWLEDGMENTS

Above all, I must give my heartfelt thanks to my advisor Dr. Tatjana Jevremovic. She has been my fiercest advocate throughout this entire process and has placed me and pushed me into numerous opportunities to learn, grow, and succeed. Many of these opportunities I would not have found anywhere else and they have set me up for success throughout the rest of my life. I know that I always had a reliable advisor to turn to for help and I will be forever indebted to her for taking a chance on me as an undergraduate engineering student. I thank my Committee, Drs. Mohanty, Ring, Guruswamy, and Beitollahi, for spending time reviewing my work and offering advice and guidance. I am grateful to Dr. Keith Prisbrey for teaching me about molecular dynamics modeling and the quantum chemistry needed to interpret results from molecular dynamics modeling. I wish to give a special thanks to Quentin Faure, Jake Tuttle, JoCee Porter, and Jean-Nicolas Dupré for assisting with experiments. Without their continued support, this research would not have been possible. I am grateful to Ryan Schow and Greg Moffitt for helping to operate the TRIGA reactor with me when necessary to perform these experiments. I am also thankful for the many students in the nuclear engineering program whom I have had the pleasure to work with, to study with, and to become friends with. Finally, I express my love and gratitude to my family, especially to my wife Kathryn, for supporting me through this journey. The journey has been long and strenuous, but we have grown together and learned together. She never gave up, never stopped encouraging me, and always made sure our home was in order so that I could finish this pursuit. My children, Rachel and Esther, while they cannot understand at this point in their lives how grateful I am for them, I still wish to thank them for always being a source of happiness and for always smiling when I needed it most.

CHAPTER 1

INTRODUCTION

Concrete has widespread use in the nuclear industry and serves several purposes. These purposes include use as biological shielding, containment structures, physical security, protection of equipment, cooling towers, spent fuel pools, and general infrastructure support. The International Atomic Energy Agency (IAEA) states that the service life for nuclear power plants was originally estimated to be 35-40 years [1]. As such, plants were designed with a useful life of 40 years. For economic reasons, many plants have had licenses extended beyond their original 40 year licenses to operate up to 60 years.

The extension of design life for nuclear power plants means that many concrete structures face ageing challenges. Concrete is inherently resistant to ageing; however, due to human error and environmental factors, it faces numerous degradation mechanisms [2]. Several different degradation mechanisms that can shorten the useful life of concrete and cause it to underperform its design specifications are outlined in Table 1.1.

Many concrete structures in the nuclear industry are of such importance that they cannot simply be torn down and replaced when they have reached the end of their useful life. Studies conducted by the IAEA and the Electric Power Research Institute (EPRI) have found that over 50% of ageing problems are due to construction deficiencies or human error [1, 2]. It follows therefore that if concrete structures cannot be replaced and if over 50% of ageing problems are due to construction deficiencies, then concrete must be improved upon at the time of placement. A period of 40-60 years into a structure's lifetime is too late to make the necessary changes to ensure safe and reliable operation of nuclear-related concrete structures. The research presented in this dissertation focuses on an advanced atomistic analysis of concrete chemistry to improve it at the time of construction. Doing so will extend its life cycle and ensure safety for 80-100 years. The goal of this research is not to address every degradation mechanism outlined in Table 1.1 but rather to improve concrete at the molecular level.

1.1 Objectives

The novel concrete chemistry is developed and analyzed in two major cases: when concrete is exposed to low gamma radiation during its curing phase, and its resistance to neutron activation during long-term exposure such as in nuclear power plants. The specific objectives of this research are as follows:

1. Improve concrete structural properties: its strength, longevity, and durability [3, 4]
2. Determine how concrete chemistry changes when it is exposed to low-dose gamma radiation during its early curing stage [3, 4]
3. Develop a concrete chemistry to ensure that concrete activation from long-term neutron flux exposure in nuclear power plants is negligible [5]

1.2 Organization of Dissertation

In Chapter 2, an improved method to curing concrete is presented using low-dose gamma radiation during the early stages of concrete curing. Chapter 3 uses Molecular Dynamics (MD) modeling to study how gamma radiation in the curing stage improves compressive strength of concrete. Chapter 4 presents a detailed methodology to control concrete chemistry at the atomistic level by assuring long-term exposure of concrete to a neutron flux in nuclear power plants will not activate above the level of low-level radioactive waste. Chapter 5 concludes the research and discusses opportunities for future work.

Table 1.1: Degradation conditions and mechanisms that affect concrete in the nuclear industry as well as the effects from the degradation conditions

Degradation Conditions	Degradation Mechanisms	Degradation Effects
Cyclic loading and unloading	Fatigue	Cracking and loss of strength
Radiation	Expansion of aggregate, internal heating	Internal cracking, loss of sterngth, water ingress
Thermal exposure	Freezing and thawing	Internal and external spallation, cracking
Foundation settlement	Uneven concrete settlement	Cracking
Reactive aggregates	Alkali-Silica-Reactions (ASR), aggregate expansion	Internal cracking, loss of strength, water intrusion
High sulfate environment	Sulfate attack	Internal and external cracking, loss of strength

CHAPTER 2

EFFECTS OF GAMMA RADIATION INDUCED FORCED FORMATION OF FREE RADICALS ON THE STRENGTH OF CONCRETE FOR USE IN NUCLEAR POWER PLANTS[1]

2.1 Abstract

In this paper, we present a summary of preliminary experiments and numerical assessments of the effects of gamma radiation induced formation of free radicals in the curing stage of concrete on its characteristics. Substantial literature reports on the damaging effects of long-term and high-dose gamma and neutron exposure on concrete. However, we show that short-term exposure of concrete to gamma radiation can be beneficial in increasing its compressive strength. The effects of exposing to 630 MBq ^{137}Cs the 56 cubes each made of 125 cm^3 concrete during the first seven days of curing are compared to another 56 cubes cured by the conventional process. The average compressive strength of the gamma cured cubes is around 8,500 psi, while conventionally cured cubes show the lower average strength of around 6,700 psi. The microstructure of the gamma and conventionally cured concrete cubes is analyzed using a scanning electron microscope. The radiolysis within the microstructure of the concrete cubes is assessed with computational modeling based on Geant4. The production of free radicals from radiolysis is shown to increase with increasing source strength and increasing the time of exposure to gamma radiation. This research shows in general that curing concrete in gamma radiation field provides observable trends toward its increased strength.

2.2 Introduction

Concrete is a composite mixture of water, cement, and coarse and fine aggregates. Cement is a fine powdery material made primarily of limestone, acting as a binder to hold the concrete mixture together. Aggregates vary widely in composition and are locally dependent, for example

[1]Steven Burnham, Quentin Faure, Michelle Tamplin, Long Huang, and Tatjana Jevremovic, "Effects of Gamma Radiation Induced Forced Formation of Free Radicals on the Strength of Concrete for Use in Nuclear Power Plants", Submitted to *Progress in Nuclear Energy*, October 10, 2016

they can be limestone or quartz based. All aggregates are generally smaller than 1.5 inches in size. Fine aggregates are generally classified as particles that pass through a 3/8-inch sieve. Aggregates account for 60-75% of the total volume of a concrete mix. Cement absorbs water; when mixed with water, a hydration process causes a formation of a gel known as Calcium-Silicate-Hydrate, or simply C-S-H [6]. The formation of C-S-H is highly amorphous and is represented by the general formula: $CaO_x \cdot SiO_2 \cdot H_2O_y$ where x and y both vary over a wide range with the calcium to silica , c/s, ratios typically between 1 and 2 [6]. Two common forms of C-S-H are the Jennite mineral $Ca_9Si_6O_{18} \cdot 8H_2O$, and Tobermorite $Ca_5Si_6O_{16}(OH)_2 \cdot 4H_2O$. The formation of C-S-H gel gives a concrete its high compressive strength in serving as a link between the aggregates and the cement paste. The force of attraction between the cement paste is attributed to the Van der Waals forces [7]. Van der Waals forces are weak intermolecular attraction forces; the electron cloud of an atom can, by chance, become concentrated in one region of an atom or molecule, thus causing a momentary polarity of an atom. This can lead to a cascading effect where other nearby atoms or molecules experience a momentary polarity. The positively and negatively charged regions can then be attracted to each other. The resultant force of attraction is weak, but taken together on a large scale, the forces can combine to be significant [8]. The attraction is the result of positive and negative polarity of molecules.

Due to its versatility, concrete is the most commonly used construction material in the world [9]. As such, concrete is very widely used in the nuclear industry both as a building material as well as a radiation shielding material. For the current Generation II fleet of the power reactors in operation, concrete is used for containment domes as well as biological shields. In the event of an accident, large containment structures made of concrete and steel are designed to reduce the radiation to the environment and reduce or stop the spread of fission products beyond the containment volume. The concrete integrity is therefore of paramount importance for continuous and sustained operation of nuclear power plants. For example, in the Crystal River Nuclear Power Plant, the concrete of the containment structure cracked on multiple occasions. This resulted in the premature closing of the nuclear power plant [10]. Newer reactors of the Generation III are built based on the Generation II technology but with improved efficiency and safety. As a result, concrete is heavily used for both biological shields and containment structures. The European Pressurized Water Reactor (EPR) uses additional concrete to protect the containment vessel. In the event of an accident, a layer of sacrificial concrete is used to catch a melting core and provide it with enough time to cool, thus protecting the overall containment structure [11, 12]. The Generation IV reactor [13, 14, 15] designs such as the sodium-cooled fast reactor, gas-cooled fast reactor, lead-cooled fast reactor, and supercritical water-cooled reactor are in various stages of the design phases [14, 15, 16], in which concrete will

still be used as a construction material for the reactor containment building and biological shields. Generation IV reactor designs have an increased focus on safety but will undoubtedly require robust containment structures in the event of a nuclear accident [15] and terrorism [17].

The main concrete property that measures the structural quality is its compressive strength. It depends on the water-to-cement ratio and the concrete curing time. Concrete compressive strength of commercial structures ranges between 3,000 and 12,000 psi while for the cast-in-place buildings, the strength usually ranges between 3,000 and 6,000 psi. The design criteria for compressive strength of concrete used in nuclear power plants' structures is defined in ACI 349-06 – Code Requirements for Nuclear Safety-Related Concrete Structures [18]. When concrete is exposed to extreme conditions such as chloride exposure, salt, or seawater, it must have a minimum compressive strength of 5,000 psi. Concrete that is exposed to less extreme environments can maintain a minimum strength of 4,000 psi[2].

The tensile strength of concrete is a measure of a structure's cracking under the load, and thus it is more important in designing highways and airfield slabs rather than a nuclear power plant's containment. It is usually defined to be 10 – 15 % of the compressive strength of concrete. For this reason, tensile strength is most often neglected in structural concrete building designs [18]. Reinforcing steel is used within concrete structures in order to accommodate for the lack of tensile strength.

There is substantial literature speaking of the damaging effects of radiation on concrete that is related to a long-term exposure of concrete to gamma and neutron irradiation in nuclear power plants. The most common elements in a concrete mix are Ca, Si, H, and O. In interacting with neutrons of low or high energies, the most probable interaction types are neutron elastic scattering and radiative capture. As a result, atoms (nuclei) in the solid lattice of concrete are dislocated; however, this defect will not accumulate in the cement portion of concrete mix due to its imperfect crystalline structure. However, dislocation of atoms in aggregates will accumulate and can cause expansion that is the reason for observed cracks in the concrete structure. This in turn affects the strength of concrete. Therefore, concrete's resistance to neutron radiation decreases with a decrease of concrete aggregates resistance to neutron exposure. It is shown in numerous studies that neutron radiation with a fluence over 10^{19} n/cm^2 may cause a noticeable increase in its volume, and therefore reduce concrete compressive strength. Due to specifics of neutron interactions with various nuclei in the concrete mix, an overall resistance of concrete to neutron radiation strongly depends on concrete mix proportions, type of a cement, and type of aggregates.

[2] 1 Psi is one pound of force acting on one square inch; 1 Psi is equivalent to 0.00689475729 MPa.

The lattice structure of the many different elements present in concrete are disordered due to gamma and neutron interactions in increasing concrete susceptibility to alkali silica reactions (ASR). Traditionally, aggregates in concrete that contain reactive silica will react with the highly alkaline environment of hydrating cement. This causes the aggregate to swell and in turn generates internal pressure within the concrete that can cause severe degradation [6]. In general, the radiation damage of the crystal lattice of otherwise unreactive aggregates has been shown to cause them to become reactive and induce ASR [19]. In order for radiation to cause damage in concrete in a measureable degree, high radiation doses of 10^7-10^{11} Gy of absorbed dose are found to be necessary [19, 20]. Therefore, the ASR can severely degrade the concrete and decrease its compressive strength.

The interaction of gamma rays or neutrons with elements in any media will result in energy transfer and therefore generation of heat. It has been previously shown that radiation can lead to an increase in temperature of an interacting medium as high as 250°C while the threshold for degradation of concrete is only 95°C [21].

Of interest to this paper is how gamma ray interactions with concrete that are studied only as a damaging effect due to long-term exposures can be beneficial when used in non-matured concrete, during its curing time. The following Section 2.5 summarizes the main effects of gamma rays in interacting with concrete, and Section 2.6 describes our experimental data on the effects of gamma rays on the curing concrete.

2.3 Effects of Gamma Rays Irradiation on Concrete Characteristics

2.3.1 Effects of Gamma Rays Induced Radiolysis of Water on Concrete

Literature indicates that long-term exposure to gamma (and/or neutron) irradiation reduces both tensile and compressive strengths as well as the modulus of elasticity of concrete structures of nuclear power installations. Specifically, a gamma dose on the order of 10^8 Gy may cause a reduction in concrete compressive strength. The most important interaction is with water in concrete that produces water radiolysis in cement paste. A consequence of this process likely causes the creep and shrinkage of concrete. As much as shrinkage is detrimental to matured concrete structures, we show in this paper that it has an incremental advantage if induced during the early development (curing) of concrete. In other words, the experimental results provided in the next section show gamma ray induced radiolysis of water during the early curing of concrete and show that the overall strength of the curing concrete may increase. The potential heating caused by these interactions show no effects to the formation of concrete and therefore its strength.

In general, a response of any composite (mixture) material to irradiation directly depends on

the responses of their components. Similarly, resistance of concrete to irradiation of any type (most important are gamma and neutron irradiation) depends directly on the resistance of the concrete's components. The most important is the effect of gamma interactions with water causing it to be decomposed by radiolysis into hydrogen and hydrogen peroxide, which in turn decompose into water and oxygen. The initial radiolytic step is described with[3] [23]:

$$H_2O \xrightarrow{\text{ionizing radiation}} e^-_{aq},\ HO,\ H,\ HO_2,\ H_3O,\ H_3O^+,\ OH^-,\ H_2O_2,\ H_2 \tag{2.1}$$

These complex species formed within concrete pores interact with themselves as well as with the elements present in aqueous solution of cement and water. Many of the products can react with each other causing recombination back to water known as back reactions. The process of radiolysis can also create products such as hydroxide that are found in Tobermorite and Jennite, two forms of C-S-H. The radiolysis of water in concrete leads to the formation of free radicals that are formed in small clusters, the spatial distribution of which is characteristic of the energy of the ionizing radiation [24]. For example, gamma induced low-energy electrons in concrete form radicals at high concentrations along a travel track. High-energy electrons form regions of low radical density. The low density allows for the radicals to diffuse and react with solutes in water [24]. In the case of concrete, they react with Ca or Si that are in the solution, thus forming these products of hydration. One scenario explaining a creation of free radicals in concrete is illustrated in Fig. 2.1.

2.3.2 Effects of Gamma Rays Induced Heating on Concrete

Exposure of concrete to heat is categorized in three fundamental ways: effects on the hydrated cement paste, effects on the aggregates, and effects on the concrete as a whole. Cement mixed with water leads to the so-called hydration process that creates the products such as C-S-H. As it forms, it traps a free water and forms capillary voids. When concrete is subjected to heat, the C-S-H begins to release that water. In a concrete that is porous, the formed steam is released from its pores. In a concrete that is denser, this formed steam has no place to go and therefore results in the formation of an internal spalling, weakening the internal structure. Very high temperatures are required to dehydrate the C-S-H. For example, at temperatures of 500°C, the C-S-H begins to dehydrate and decompose with its full decomposition starting at around 900°C [7]. Hydration of cement is an exothermic reaction producing up to 500 J/g cement [25]. In most instances, the heat is able to be transferred to its surroundings. Large concrete structures can present challenges due to the low thermal conductivity of concrete. It can act as an insulator and the interior body of the concrete can

[3] The term e^-aq refers to the initial free electron produced through the interaction of a gamma ray with a water molecule. This electron is captured by a water molecule and becomes solvated, being referred to as an aqueous or solvated electron. The solvated electron can react with H^+ to form the hydroxyl radical [22].

see a rise in temperature greater than 55°C [25, 26]. Instances where there is a large increase in temperature can cause the concrete to expand and then contract nonuniformly, causing premature cracking and internal stresses [26]. The heat of hydration can be mitigated by slowing the hydration process and allowing for dissipation of heat. This is accomplished using the so-called set-retarding admixtures [7]. Accelerating the hydration process too much, however, can cause excessive internal heating even in small structures that might not otherwise be affected by the heat of hydration.

The effects of heat on the aggregates in concrete are similar to hydrated cement paste. Porous aggregates have their water converted to steam. In a low porosity environment, the steam will create internal pressure and cause the aggregate to crack and lose strength. Other specific types of aggregate can have varying effects. Granite and sandstone that are high in silica will undergo a phase change at 573°C that causes sudden expansion [7]. An expansion of aggregate causes increased pressure within the entire concrete structure forming cracks. The cracks will weaken the bond between the aggregate and hydrated cement, thus decreasing compressive strength.

The effects of heating on both the hydrated cement and aggregate combine to affect concrete in a negative manner. It was demonstrated [27] that concrete exposed to temperatures over 800°C for even a short duration of time can reduce 40% of its strength.

Radiation heating of concrete can also have negative effects in the form of both shrinkage and expansion [28]. As stated earlier, when the hydrated C-S-H is heated, the internal water is released in the form of steam. This process causes the C-S-H to lose its volume. On the other hand, the aggregate can expand as a result of its lack of porosity not allowing the water to escape as easily. Larger aggregate sizes create a mismatch in size with the shrinking C-S-H resulting in less surface area contact and decreasing the overall strength on the concrete mix.

The amount of heating generated due to gamma rays interaction with any material can be approximated by taking into account the energy absorbed by the material (absorbed dose) and the specific heat capacity of the material, as follows [29][30]:

$$Q = c\Delta T \tag{2.2}$$

where

$Q =$ energy absorbed or absorbed radiation dose by a material $(\mathrm{J/g})$

$c =$ specific heat capacity of a material or the energy required to raise the temperature by $1^{\circ}\mathrm{C}$ $(1\mathrm{J/g}^{\circ}\mathrm{C}$ for fresh concrete, determined experimentally $)$

$\Delta T =$ change in temperature of the material absorbing radiation $(^{\circ}\mathrm{C})$

For example, if a fresh concrete mixture is exposed for seven (7) days to a ^{137}Cs source of intensity of 630 MBq, corresponding to absorbed dose of 0.746 J/kg, it follows that increase in concrete internal temperature due to gamma ray interactions is negligible:

$$\Delta T = \frac{7.46 \times 10^{-4\,J/g}}{1\,J/g°C} = 7.46 \times 10^{-4}°C \tag{2.3}$$

2.4 Effects of Gamma Radiation on Concrete Characteristics During Its Early Stage of Curing

This section describes the experiment we have developed to assess if the curing concrete exposed to gamma rays develops with enhanced strength and to understand what processes may be responsible for such a finding.

2.4.1 Experimental Setup to Gamma Curing Process

Based on the process of radiolysis of water within concrete (described in Section 2.1) as well as on understanding some of the known structures of C-S-H gel, we explored the possibility that short-term exposure of concrete to gamma radiation can enhance the curing phase and lead to its increased strength. In the experiment, we exposed curing concrete in a controlled environment (temperature and humidity) to a ^{137}Cs source for the first seven days after it was mixed. The concrete mixtures were controlled to ensure consistency among the concrete cubes within accepted laboratory practices. The experiment included:

• Measuring the absorbed radiation dose to concrete cubes exposed to a 630 MBq ^{137}Cs source for seven (7) days. A ^{137}Cs source was chosen because it is a mono-energetic source emitting a single 662 keV gamma ray. The activity of 630 MBq was chosen based on source availability in our laboratory and it has been chosen to not be too weak and not be too strong.

• Measuring the compressive strength of gamma cured versus conventionally cured concrete after seven (7) days of curing.

• Analyzing the changes in the microstructure of concrete cubes in relation to the measured compressive strength.

• Analyzing if gamma heating causes any micro or macro structural changes within the concrete cubes.

• Determining the rate at which free radicals are produced within the micro pores of concrete and their correlation to concrete strength.

Several batches of the same concrete mixture were developed in the laboratory of the Utah Nuclear Engineering Program during the months of February and March, 2016 with the following content: 0.4 water to cement (w/c) ratio with only fine aggregates (sand) mixed in a 2.75 sand

to cement (s/c) ratio. Procedure for mixing the concrete cubes is outlined in ASTM Standard C192/192M – Making and Curing Concrete Test Specimens in the Laboratory [31]. Due to the fineness of the aggregates used, concrete cubes of 125 cm^3 in volume are cast and used for the compressive strength testing. The ASTM C192/192m procedure is followed, but concrete cubes are demolded after only five (5) hours of curing time, because we were testing the effects of gamma radiation on concrete during the very early stages of curing. Therefore, the test cubes were demolded as soon as they were able to hold their form on their own and thus be placed in the gamma irradiator. After demolding, both sets of concrete cubes are cured in dry air for a period of seven days. One set was exposed to a 630 MBq source during the entirety of the seven days while the other set of concrete cubes was not exposed to any radiation other than naturally occurring background radiation.

Although preliminary analytic estimates show that exposure of concrete to 630 MBq ^{137}Cs source for seven (7) days will not generate any excess heat within the concrete (Section 2.2), we also examined if gamma heating would be generated in the concrete cubes in any observable way and compared it to the effects that heat may produce as follows: one set of cubes was cured in dry air and exposed to the same 630 MBq source, while the second set was cured in dry air with no exposure to this same source. Additionally, a third and fourth set of cubes was cured in an oven: one set at 95°C and the other at 120°C.

2.4.2 Gamma Rays Absorbed Dose Within the Concrete Cubes: Experimentally Measured and MCNP6 Estimated

The absorbed dose due to gamma ray interactions within the concrete cubes was both calculated and determined experimentally.

The exact experiment layout is shown in Fig. 2.2. (a), while the MCNP6 model of the experiment is shown in Fig. 2.2. (b). As can be seen, the isotropic ^{137}Cs source with gamma energy of 662 keV is placed in the center of the 12 125 cm^3 volume concrete cubes.

2.4.2.1 MCNP6 values

In general, when using MCNP6 (Monte Carlo N-Particle) [32], the absorbed radiation dose is calculated using the F6 tally. The absorbed dose is obtained to be 66 cGy for the concrete cubes exposed for seven days to a ^{137}Cs 630 MBq source. Figure 2.3 shows the absorbed dose map, based on calculated and measured values. It can be seen that the calculated dose is the same for every concrete cube. This is because the MCNP6 geometry is perfectly symmetrical, the isotropic ^{137}Cs source is located exactly in the center with all cubes located at the exact same distance from it. In the experiment, however, the position of the source and the cubes are not as perfect and the discrepancy in the dose values is therefore expected (as explained below).

2.4.2.2 Experimental values

A Landauer nanoDOT [33] system is used to measure the absorbed dose in the concrete cubes (Fig. 2.2 (a)). The nanoDot system is known to have a linear response up to 3 Gy of exposure and is accurate to within 5% for an energy range of 5 keV to 20 MeV [33]. The nanoDots used in this experiment were previously used and therefore were irradiated but had only accumulated a dose of 1.5 Gy or less. The low dose accumulation provided assurance that they will be suitable for further use since the total cumulative dose will not exceed 3 Gy. The linear response of the nanoDots was verified by exposing three nanoDots to 1 Gy from a 6 MV x-ray source. An additional three nanoDots were also exposed to a dose of 2 Gy from the same 6 MV x-ray source. The experiment layout is shown in Fig. 2.4. The total cumulative dose is then measured to test the linear response and accuracy of the measurement when the nanoDots are reused. Two nanoDots are placed on the front and back of each of the concrete cubes prior to exposure to the ^{137}Cs source. The measured dose of the nanoDots indicated that the dose response was linear as expected and accurate, making the nanoDots suitable for re-use. The dose response is then tested by exposing the nanoDots to the 630 MBq ^{137}Cs source. Four nanoDots with accumulated dose from previous experiments were placed on the front of a concrete cube as shown in Fig. 2.5. The dose to each of the nanoDots is measured and the initial dose is subtracted from the total cumulative dose to determine the total exposure to each of the nanoDots. The average absorbed dose was 74.6 cGy. Table 2.1 shows the measured dose values for each of the nanoDots. The measured dose is also compared to the MCNP6 calculated dose of 66 cGy. Table 2.1 shows that the nanoDots responded correctly after exposure to a 630 MBq ^{137}Cs source for seven days making them accurately suitable for the use in this experiment.

The absorbed dose was measured for two different concrete cube mixes: the first consisting of six cubes made of only water and cement (cement paste) at a proportion of 0.4 w/c as stated earlier, and the second consisting of six cubes where sand was added at a ratio of 2.75 s/c. On each of the twelve cubes, two nanoDots are placed at the side directly facing the ^{137}Cs source and two are placed on the rear face directly opposite, shown in Fig. 2.6. After seven days of exposure, the dose to each of the nanoDots was measured. The dose of each nanoDot on the rear face was subtracted from the measured dose of the nanoDot on the front face of the concrete cubes to obtain the total dose absorbed by the concrete cubes itself.

Cement paste cubes 1, 2, and 3 (see Fig. 2.3) received absorbed doses higher than cubes 4, 5, and 6. This is explained by the slightly off center position of the ^{137}Cs source, making it closer to cubes 1, 2, and 3 and further away from cubes 4, 5, and 6. Cubes 5-10 most closely match the distance of the ^{137}Cs source in the MCNP6 simulation of 11 cm. This is reflected in that they also most closely match the calculated dose rates shown in Fig. 2.3. Those cubes that were closer to the

source as a result of it being placed slightly off center had higher absorbed dose rates. The average absorbed dose to the sand and cement cubes is found to be 69.1 cGy while the average of the cement cubes is found to be 85.5 cGy. These values are compared to an MCNP6 calculated value of 66 cGy. The sand and cement cubes (7-12) are generally closer to the 11 cm distance of the source in the MCNP6 model while the cement cubes (1-11) are even closer to the source, causing a higher average absorbed dose. The absorbed dose values for all 12 cubes are shown in Table 2.2.

2.4.3 Comparison of Compressive Strength Between the Gamma Cured and Conventionally Cured Concrete Cubes

Compressive strength testing is performed on only the sand and cement cubes according to the proportions and time frame outlined in Section 3.1. The sand and cement mixtures more accurately represent the concrete mixtures used in construction. The cubes that were used in the dose measurement experiment were not tested for compressive strength. During the placement and removal of the OSLDs, the cubes became too damaged to accurately test for compressive strength. As a result, a total of 120 concrete cubes from five separate batches of concrete cube mixes are tested for compressive strength. Each batch consisted of 12 cubes marked for gamma curing and 12 cubes marked for conventionally curing. Occasionally, a few cubes from each batch would stick to the molding and become damaged in such a way that they had to be discarded. This occurred in batches 4 and 5 of both the gamma cured and conventionally cured cubes. In total, 112 cubes were tested for compressive strength. Half of the cubes (56) are gamma cured while the other half are conventionally cured. Compressive strength testing is performed in the University of Utah Structures Laboratory using an INSTRON universal testing machine [34] with computer controlled loading rate. All testing is performed in accordance with ASTM standard C109 – Standard Test Method for Compressive Strength of Hydraulic Cement Mortars [35]. Each of the cubes is loaded into the INSTRON machine applying a loading rate of 200 lb/s in accordance with ASTM C109. The compressive strength of each cube is shown in Fig. 2.7.

The average compressive strength of the gamma cured concrete is 8,563 psi while the average compressive strength for the conventionally cured concrete is 6,710 psi. A t-test[4] is performed to compare the gamma cured cubes to the conventionally cured cubes in order to analyze the closeness of the two data sets. The resultant p-value[5] from the t-test is 1.26×10^{-12}, indicating that the two data sets are dissimilar and the overall compressive strength of the gamma cured concrete is higher than

[4] A t-test is a statistical test used to compare different sets of data in order to determine if they are the same or significantly different from each other.

[5] The p-value represents the probability from the t-test that the two data sets being compared are the same.

the conventionally cured cubes. The gamma cured cubes also exhibited a lower average standard deviation (405.4 psi) compared to the conventionally cured cubes (592.04), indicating greater consistency in each of the batches when gamma cured. The only exception is batch E where the gamma cured had a standard deviation of 481 psi while the conventionally cured had a standard deviation of 401 psi. The average compressive strength of batch E of the gamma cured (9,700 psi) is still higher than the average compressive strength of batch E of the conventionally cured (8,430 psi). It is anticipated that with more testing, the majority of the batches will follow the trend of having both a lower standard deviation and higher average compressive strength and that batch E will be shown to be an anomaly.

2.4.4 Analysis of the Concrete Cubes Micro Structure Using the Scanning Electron Microscope (SEM)

The crushed remains of the concrete cubes from batch E (11 gamma cured and 11 conventionally cured cubes) are collected and sealed in plastic bags after compressive strength testing for analysis using SEM. In the Crus Advanced Materials Technology Center at the University of Utah, a Hitachi S-4800 SEM is used to examine the microstructure of the concrete cubes in order to correlate the difference in their compressive strength values (batch E, as shown in Fig. 2.7). The compressive strength of the gamma cured and conventionally cured cubes from batch E shown in Fig. 2.7 are shown in greater details in Fig. 2.8. The microstructure of the gamma cured concrete cube with the highest compressive strength of 10,662 psi, concrete cube 8 shown in Fig. 2.8(a), and the microstructure of the conventionally cured concrete cube with the highest compressive strength of 9,396 psi, concrete cube 11 shown in Fig. 2.8(b), is compared. The SEM images of these two cubes are shown in Fig. 2.9. Both cubes are similar in showing a low void ratio. The void ratio is represented by the dark areas in the SEM images. A lower void ratio means that there is more contact between the C-S-H and the aggregate, causing an increase in strength.

The concrete cubes from batch E with the lowest compressive strength as shown in Fig. 2.8 (gamma cured concrete cube 10 with compressive strength of 8,378 psi and conventionally cured concrete cube 1 with compressive strength of 7,528 psi) are also compared using the SEM and the images are shown in Fig. 2.10. Both cubes show similar SEM images with a low void ratio and well-developed C-S-H.

From these SEM image analyses, it appears that the gamma and conventionally cured concrete are shown to be similar in their void ratios as well as their development of C-S-H for both the cubes with high and with low compressive strength. The analysis suggests that for short-term exposure to gamma radiation and absorbed gamma doses of less than 1 Gy (Fig. 2.3), no significant or visible changes occur to the microstructure of concrete. The lack of change in the microstructure suggests

that the increase in strength observed in the gamma cured cubes is likely due to changes occurring at the molecular level and interactions taking place between free radical formation and the products of hydration formed during the early curing stages. The complexity of C-S-H is not well understood [36]. The SEM analysis is only able to provide visual structure of the concrete at the micro level. Our future research, already on-going, is addressing this issue.

2.4.5 Effects of Gamma Rays Induced Heating on Concrete Microstructure

Gamma radiation cured concrete cubes are also compared to cubes that are cured in a high temperature environment in order to assess if the analytical estimates (Section 2.2) compared to the experiment. As described in Section 2.4.1, heat can cause damage to concrete at temperatures as low as 95°C. The same concrete mix as described in Section 2.4.1 is used to analyze the effects of high temperature on the microstructure using SEM. The SEM images are then compared to those of the gamma cured cubes in order to compare if any gamma heating may be taking place. Twelve concrete cubes are cured using gamma radiation in the same manner as described in Section 2.4.1. Eleven cubes are cured in an oven at 95°C, while six (6) cubes are cured in the oven at 120°C. The number of cubes in each batch is dependent on the number of concrete molds available in the laboratory at the time of mixing. The two temperatures were chosen based on a literature survey [21] indicating that the damage to concrete can occur at temperatures at and above 95°C. A slightly higher temperature of 120°C was also chosen since it is high enough above the boiling point of water that dehydration and steam formation within the pores is expected to be therefore accelerated. A batch of six (6) cubes is used as a control and they are cured in dry air at 23°C with no exposure to radiation and are mixed according to the same standards as described in Section 2.4.1. All cubes are tested for compressive strength using the same method as described in Section 2.4.3. The crushed cubes are then saved for SEM analysis. The measured compressive strength is shown in Fig. 2.11. The compressive strength of the gamma cured cubes is compared to the cubes cured in the oven, and control cubes, using a t-test. The resultant p-values for the gamma cured compared to the heat cured concrete cubes at 95°C, 120°C, and the control at 23°C are 0.025, 0.069, and 0.04, respectively. These p-values indicate that the gamma cured cubes still exhibit a higher overall compressive strength than those cured using heat or the control set.

The microstructure of the concrete cubes with the highest compressive strength from batches A, B, and C (Fig. 2.11) are shown in Fig. 2.12. These are cubes 6 (batch A, gamma cured), 1 (batch B, heat cured at 95°C), and 1 (batch C, heat cured at 120°C). The gamma cured and heat cured cube at 95°C are nearly identical in appearance having small voids with well-developed C-S-H. The heat cured cube at 120°C has C-S-H in similar appearance but has one large void that may be a result of greater dehydration due to the elevated temperature.

The cubes with the lowest compressive strength are also compared as shown in Fig. 2.13. From Fig. 2.11, these are cubes 5, 10, and 6 for the gamma cured (batch A), heat cured at 95°C (batch B), and heat cured at 120°C (batch C), respectively. Similar to the cubes with the highest compressive strength, the gamma cured and heat cured at 95°C exhibit comparable features with a low void ratio and well-developed C-S-H. The cube cured at 120°C also has features similar to cube 1 which has the highest compressive strength as shown in Fig. 2.13(c).

In Section 2.3.2, it was shown that the gamma source used for this experiment does not cause any significant change in temperature in the concrete cubes. From the SEM analysis comparing gamma and heat cured concrete cubes, it is shown that even if heating is to occur to a degree that damage has been shown to occur [23] (>95°C), seven days is not enough time to disrupt the microstructure within the concrete cubes.

2.5 Geant4 Simulation of Free Radical Formation Within Concrete

To better understand the radiolysis occurring within the micropores of the gamma cured concrete, Geant4 [37] is used to simulate the formation of free radicals as well as the rate at which they are formed. The chem2 example provided in the Geant4-DNA toolkit [38, 39] is used as a base for this simulation. The chem2 module simulates radiolysis and its associated reactions. The material definition of the world is set to portland cement and water at a w/c ratio of 0.4. Porosity is simulated by homogenously distributing water in a volume of portland cement. A porosity value of 14% is used based on literature values for a 0.4 w/c mix ratio [40]. The geometry accurately replicates the laboratory experiment in Fig. 2.2, a 125 cm^3 cube composed of cement and water and placed 11 cm from a ^{137}Cs source. The Geant4 model is shown in Fig. 2.14. Three different source strengths of 37 MBq, 630 MBq, and 1,260 MBq with four different exposure times of one hr, 12 hr, one day, and seven days is simulated. The total production of free radicals in moles/s is shown in Figures 2.15-2.17.

The simulation shows that as both time of exposure and source strength increases, the production of free radicals also increases. Free radical production does, however, begin to taper off with increasing time and source strength. The difference between seven days of exposure at 630 MBq and 1,260 MBq is not twice as much, despite the source strength being twice as strong. This suggests that the benefits of increased strength from gamma curing might also begin to taper off and a source twice as strong may not offer any increased benefit. The free radical production also begins to taper off with time of exposure. The results support the idea that gamma exposure is most beneficial during the early stages of curing.

2.6 Conclusion

Substantial literature documents how both gamma and neutron radiation have degrading effects on concrete over time periods of several decades of exposure. The C-S-H, a product of hydration within concrete, acts as a binder for all the concrete constituents. Radiation can cause heating within the internal concrete structure and cause the C-S-H to dehydrate and lose its strength. The process of dehydration from radiation can be caused by two mechanisms: gamma heating and radiolysis. Dehydration of C-S-H causes shrinkage and therefore a loss in volume. The shrinking C-S-H has less surface area to bond to aggregates, creating an overall decrease in overall strength of the concrete. Heat can also cause internal stress in aggregates as the water contained in their pores is converted to steam. The internal pressure causes cracking and a loss of strength. The structure of C-S-H can vary widely and exists in many forms such as Jennite and Tobermorite. When gamma rays interact with water, radiolysis will occur, forming free radicals such as H^+ and OH^-, the formation of which may be beneficial to concrete's compressive strength. We presented the results of short-term gamma radiation exposure to concrete during its first seven days of curing, and how its properties change. A 630 MBq ^{137}Cs source is shown to provide a calculated dose of 0.66 Gy and an average measured dose of 0.75 Gy to concrete cubes 125 cm^3 over seven days of exposure. The dose is calculated with MCNP6 and determined experimentally. A slight difference between the calculated and experimental doses is due to the off center positioning of the ^{137}Cs source in the experiment, causing a higher dose in some of the concrete cubes. The dose is substantially less than required to damage to concrete. The compressive strength of gamma cured and conventionally cured concrete cubes is compared showing that gamma cured cubes have an average compressive strength of 8,563 psi compared to conventionally cured cubes with average compressive strength of 6,710 psi. The gamma cured cubes also exhibited a lower standard deviation than the conventionally cured cubes. The SEM analysis of the microstructure of the gamma and conventionally cured cubes yielded no discernable difference between the two, suggesting that changes most likely are taking place at the atomistic level. A possible explanation is the process of radiolysis that creates an excess of H^+ and OH^- promoting formation of C-S-H more quickly. A more rapid formation of C-S-H thus may cause better bonding between the aggregates at an earlier stage of concrete curing. The formation of free radicals within the microstructure of concrete cubes was analyzed also with Geant4 computational modeling. Increasing source strength and time of exposure shows an increase in the rate of free radical productions. It is, however, shown that after seven days of exposure to 630 MBq gamma source, the increased rate of production is minimal. The results support the idea that the benefits of gamma curing are most beneficial during the first seven days of curing. Future testing is planned to include curing cubes for 28 days in comparison to conventionally cured concrete cubes, to analyze if

the benefits do diminish over time. Additionally, molecular dynamics simulation of concrete under these conditions is underway.

2.7 Acknowledgements

This research is supported by the Utah Nuclear Engineering Program, and the US NRC fellowship grant. The authors are thankful to Dr. Bill Salter of the Huntsman Cancer Institute at the University of Utah for assisting in the experiments as presented in this paper.

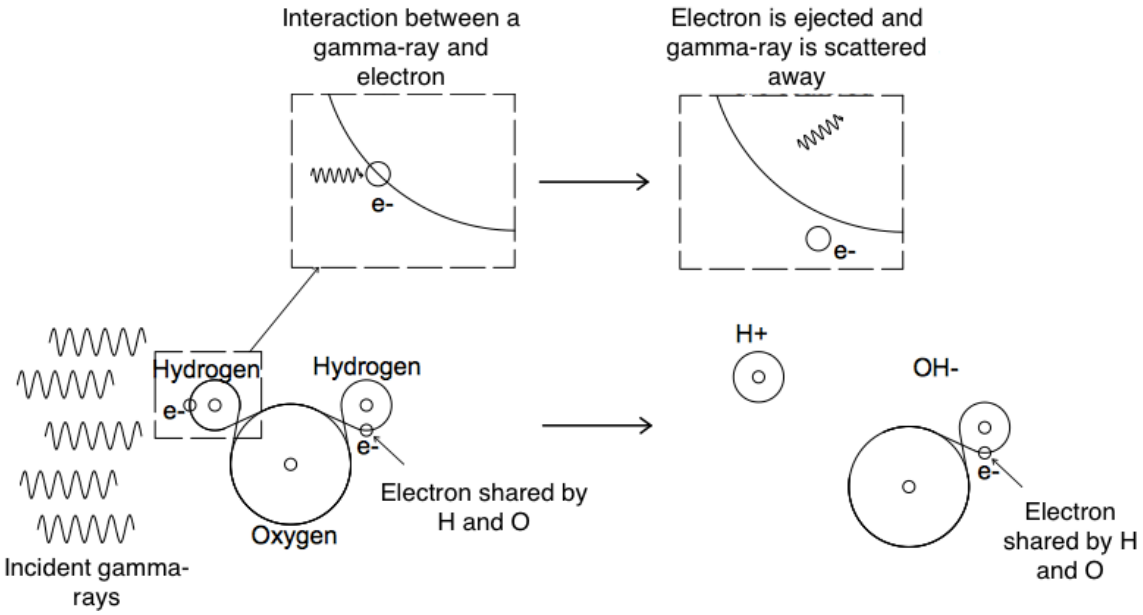

Fig. 2.1: Scenario in which H^+ and OH^- are formed from Compton scattering of a gamma ray with a water molecule in concrete mixture.

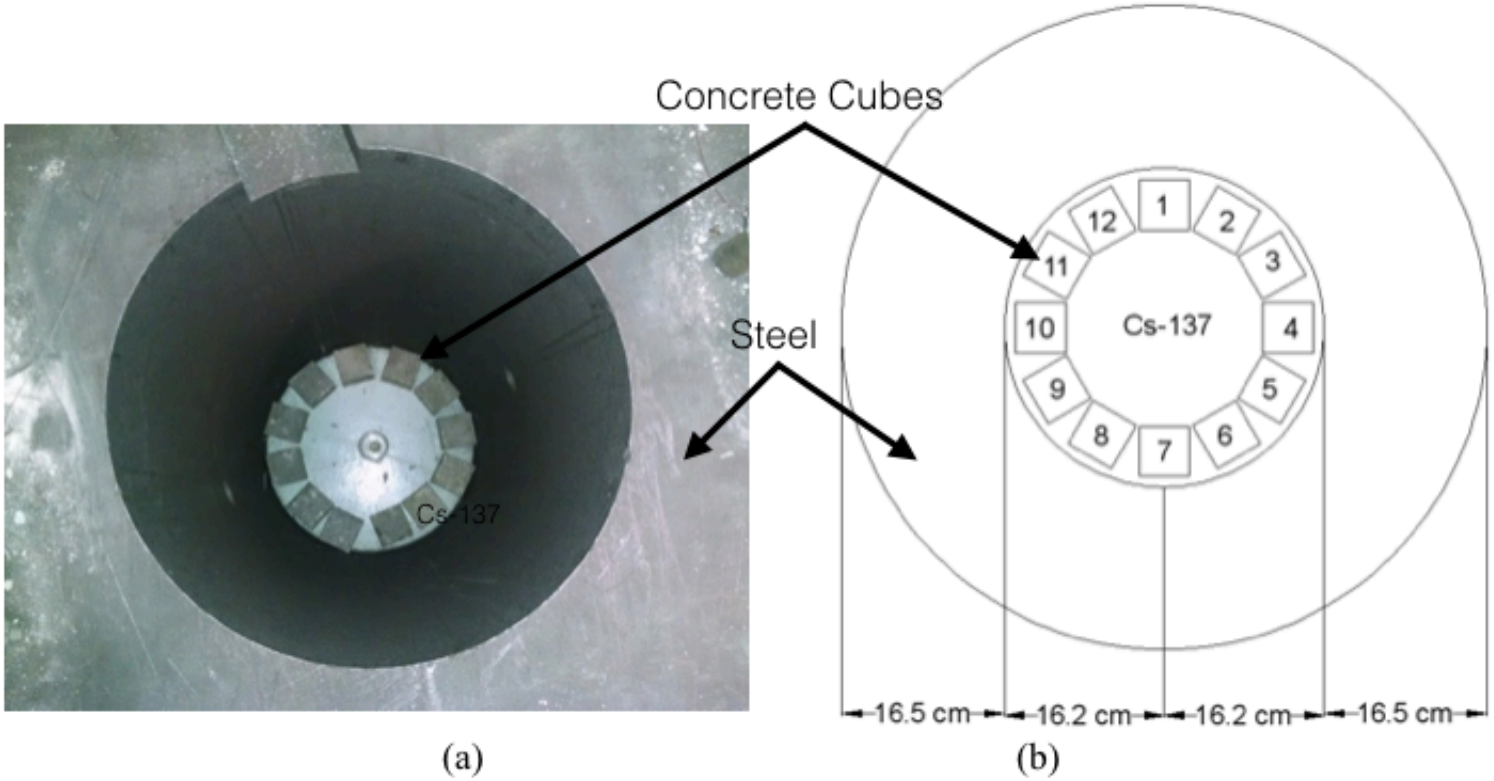

Fig. 2.2: Experimental setup (a) for gamma curing and MCNP6 model (b) for calculating absorbed gamma ray dose to concrete cubes.

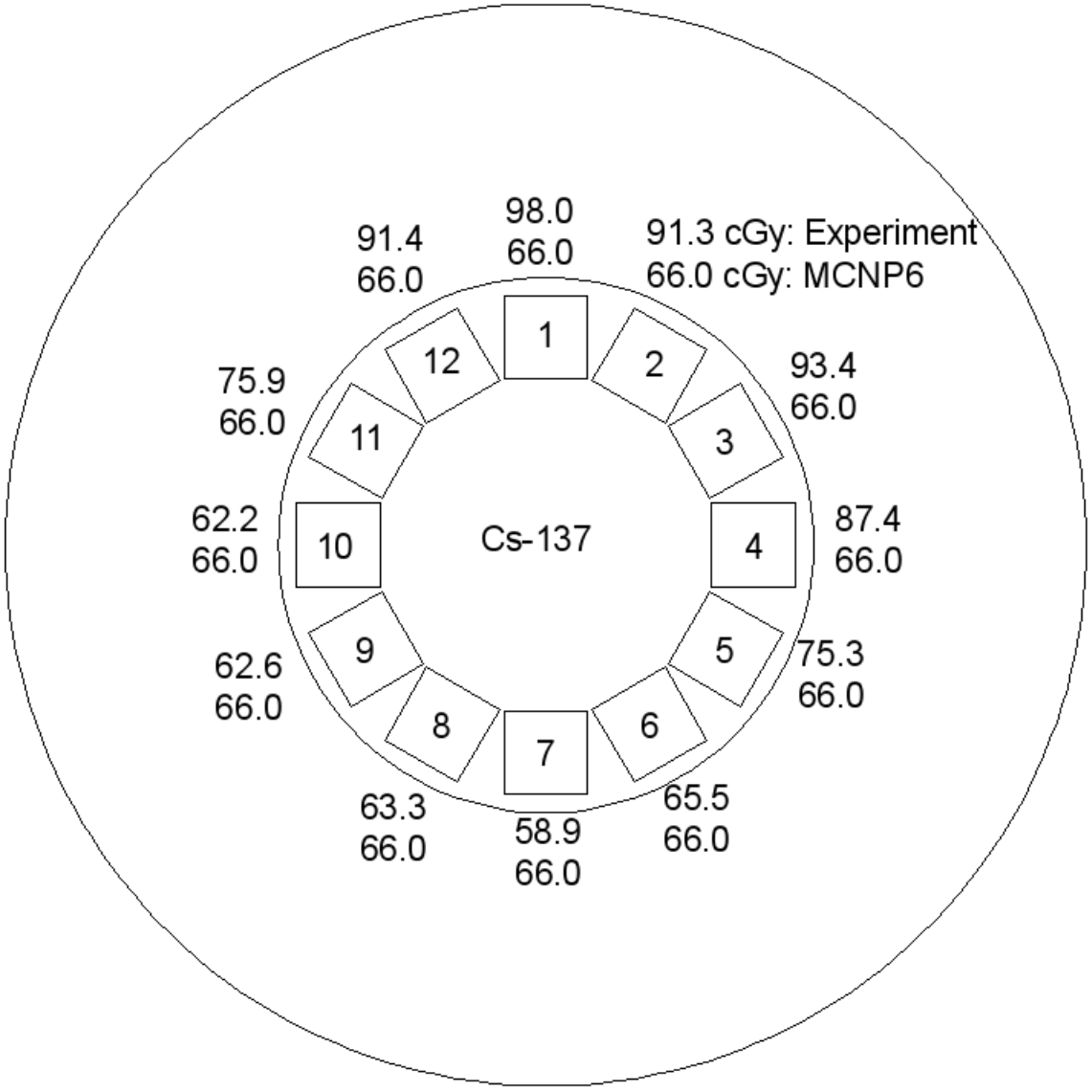

Fig. 2.3: Experimental and MCNP6 absorbed dose values due to gamma exposure to concrete cubes [The MCNP6 calculated absorbed dose for each cube is the same because the ^{137}Cs isotropic source is placed exactly in the center of all the concrete cubes. In the experimental setup, the source was not located as precisely at the center as in the MCNP6 model, thus the values of absorbed dose vary].

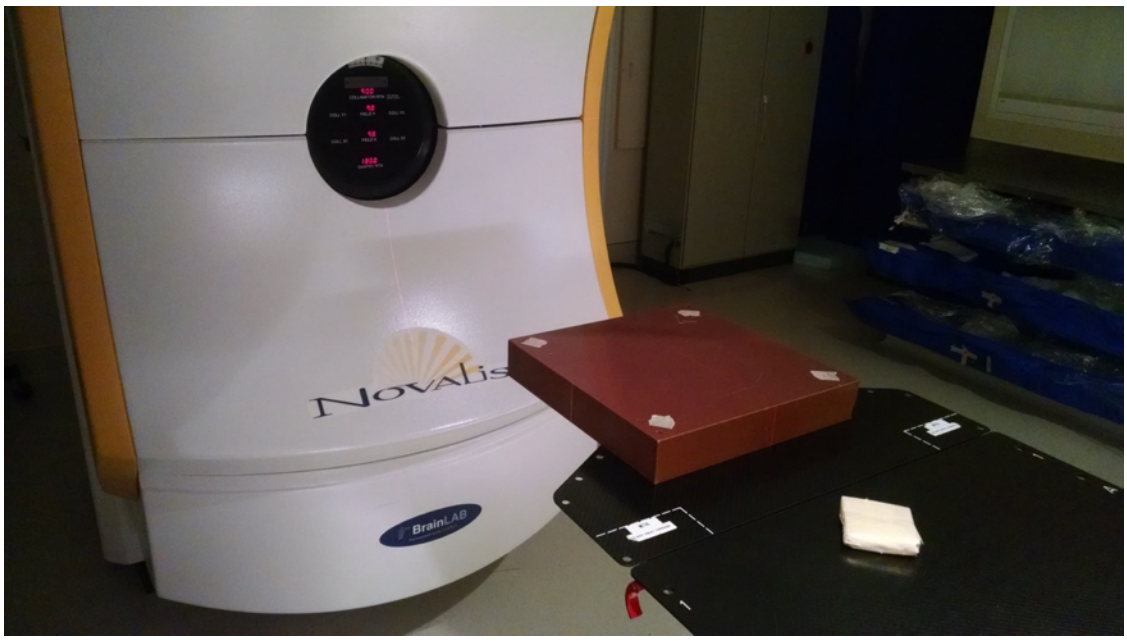

Fig. 2.4: Experimental measurement of the cumulative radiation dose response of Landauer nanoDots with a 6 MV x-ray source.

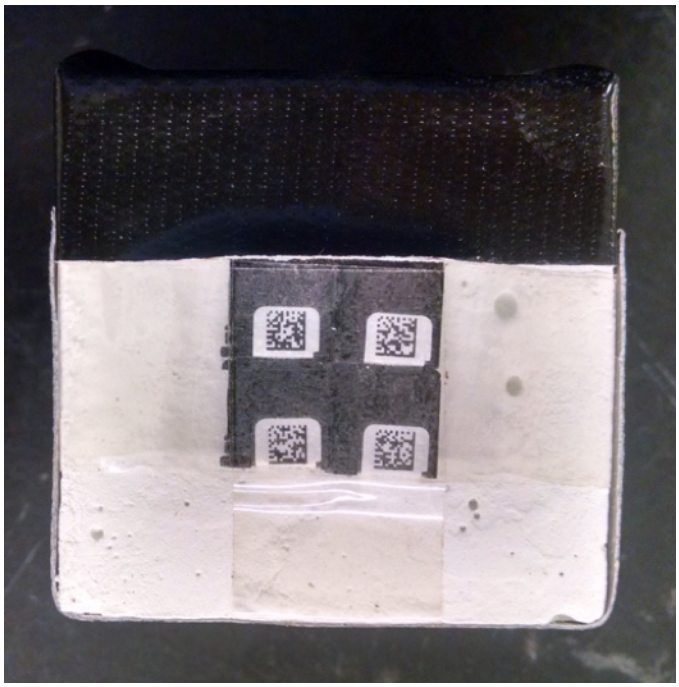

Fig. 2.5: Concrete cube with nanoDots placed on the front face for dose measurement from exposure to ^{137}Cs source.

Table 2.1: Absorbed dose of four nanoDots from exposure to ^{137}Cs source.

nanoDot	Starting Dose (cGy)	Measured CumlativeDose (cGy)	Measured Cumulative Dose–Starting Dose (cGy)
1	112.733	186.119	73.385
2	84.756	159.043	74.287
3	120.163	192.648	72.485
4	149.549	227.861	78.312

Fig. 2.6: Concrete cube with two nanoDots for absorbed dose measurement.

Table 2.2: Measured absorbed dose in cement paste cubes and sand and cement cubes

Mixture	Cube	Front Cube Dose (cGy)	Back Cube Dose (cGy)	Front Cube Dose Minus Back Cube Dose (cGy)
Cement Paste	1	136.6	38.6	98.0
	2	127.2	35.9	91.3
	3	125.7	32.2	93.4
	4	120.0	32.6	87.4
	5	103.4	28.1	75.3
	6	94.7	29.3	65.5
Sand and Cement	7	85.1	26.2	58.9
	8	89.2	25.8	63.3
	9	90.0	27.4	62.6
	10	91.6	29.5	62.2
	11	106.0	30.1	75.9
	12	124.4	33.0	91.4

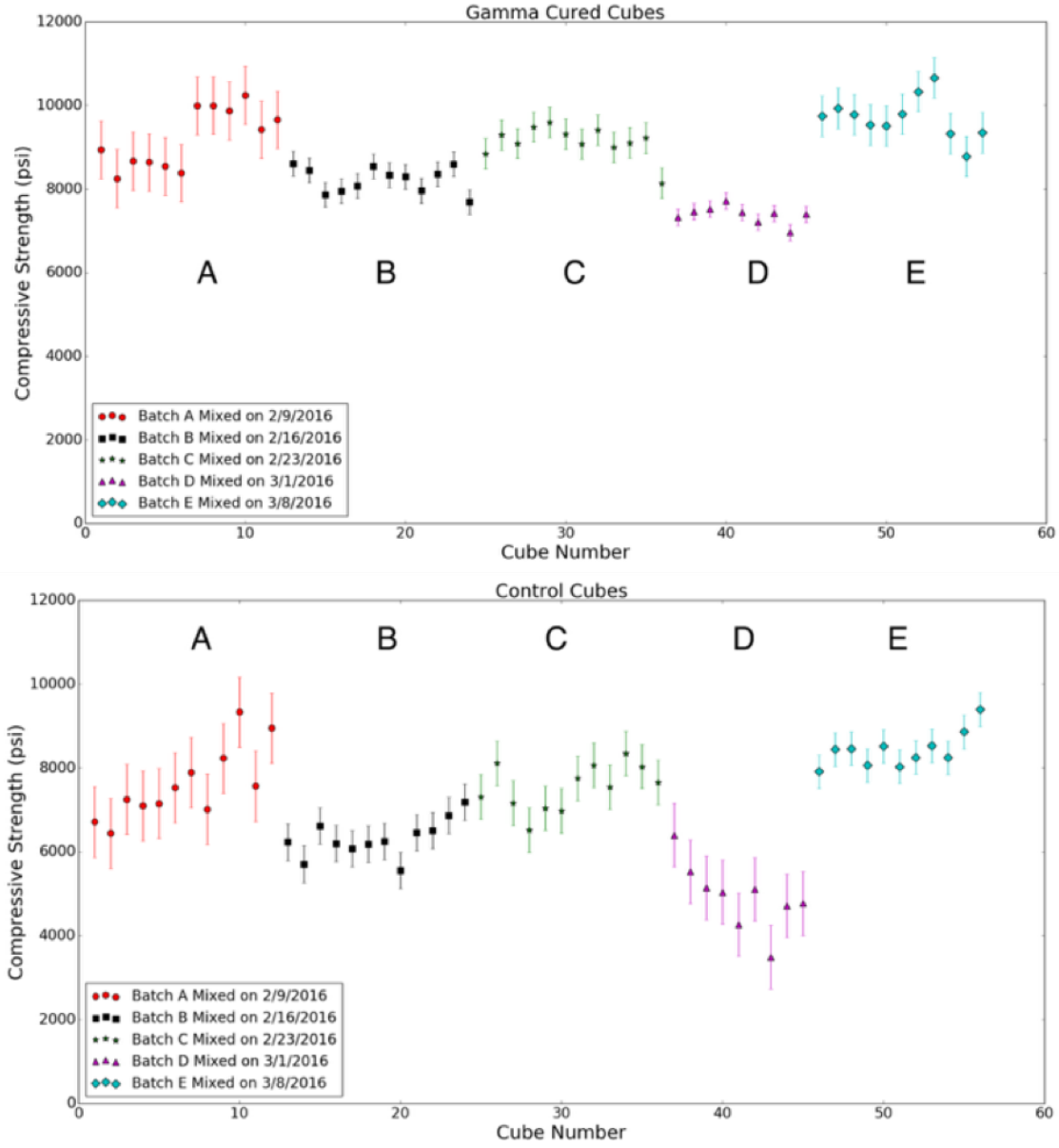

Fig. 2.7: Compressive strength of gamma cured (top) and conventionally cured (bottom) concrete cubes. The five batches labeled A-E are mixed between the months of February – March, 2016.

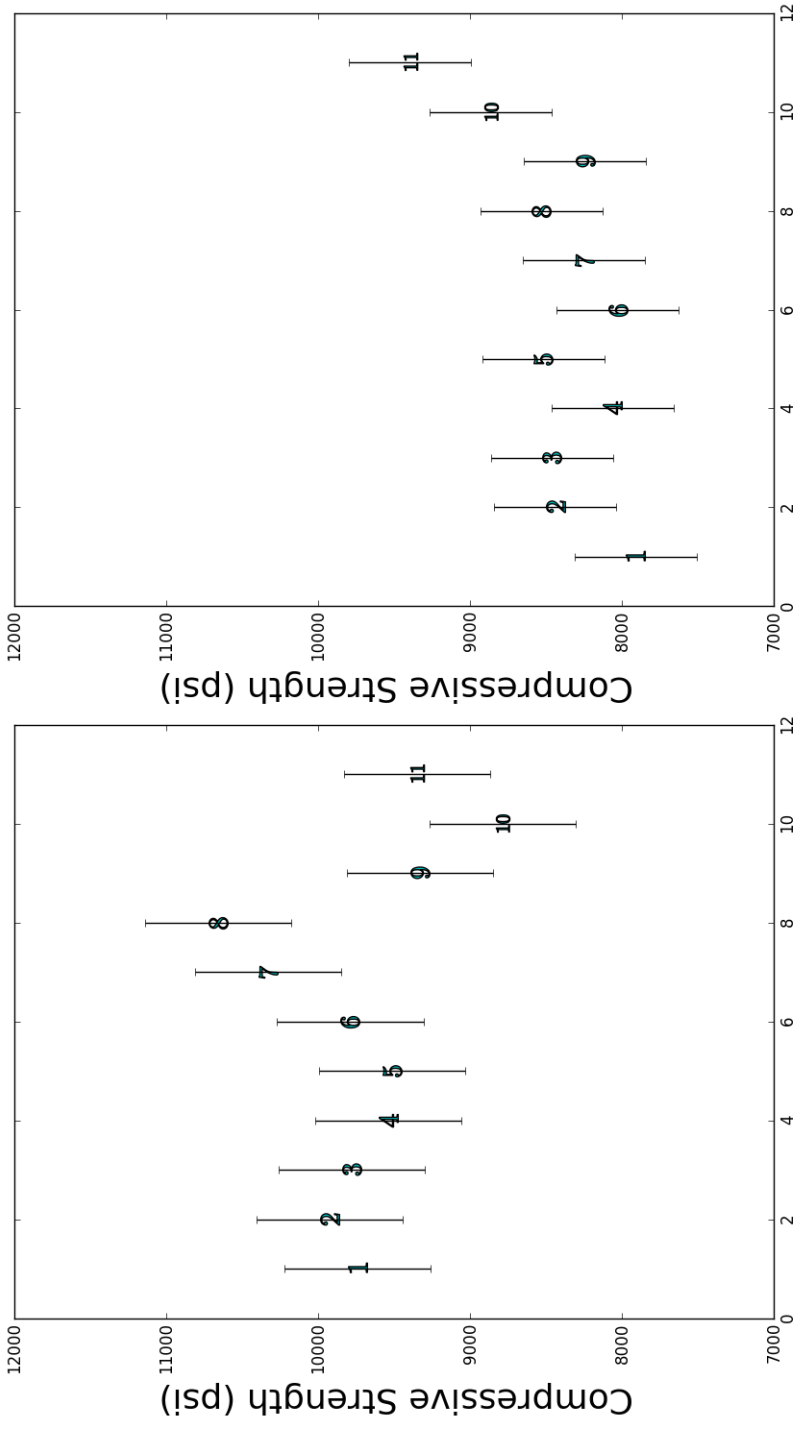

Fig. 2.8: Detailed view of the compressive strength of batch E of (a) gamma cured and (b) conventionally cured concrete cubes (mixed on 8 March 2016).

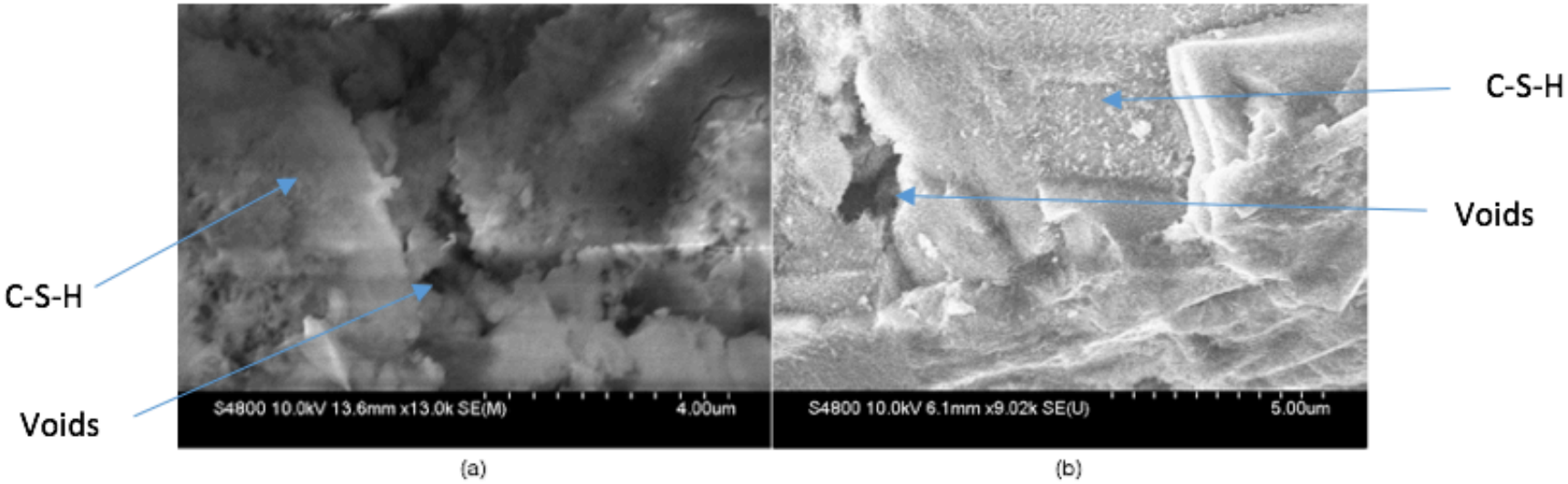

Fig. 2.9: SEM images of (a) cube 8 of Fig. 2.8(a) (gamma cured) and (b) cube 11 of Fig. 2.8(b) (conventionally cured) concrete cubes with the highest compressive strength as shown in Fig. 2.8.

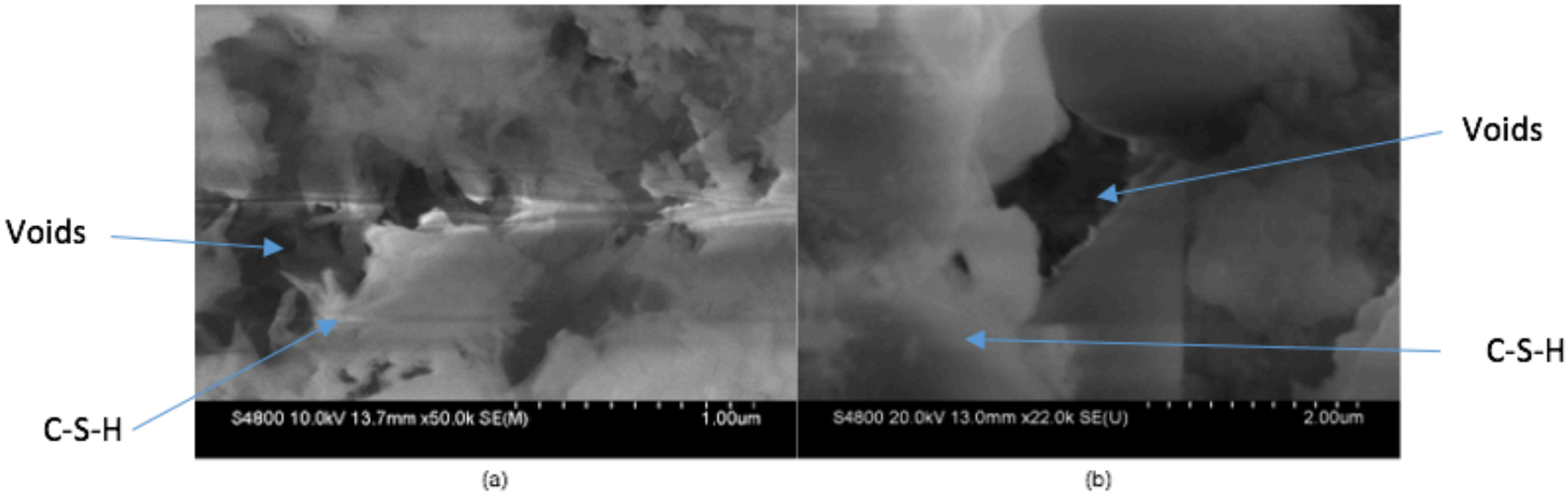

Fig. 2.10: SEM images of (a) cube 10 of Fig. 2.8(a) (gamma cured) and (b) cube 1 of Fig. 2.8(b) (conventionally cured) concrete cubes with the lowest compressive strength as shown in Fig. 2.8.

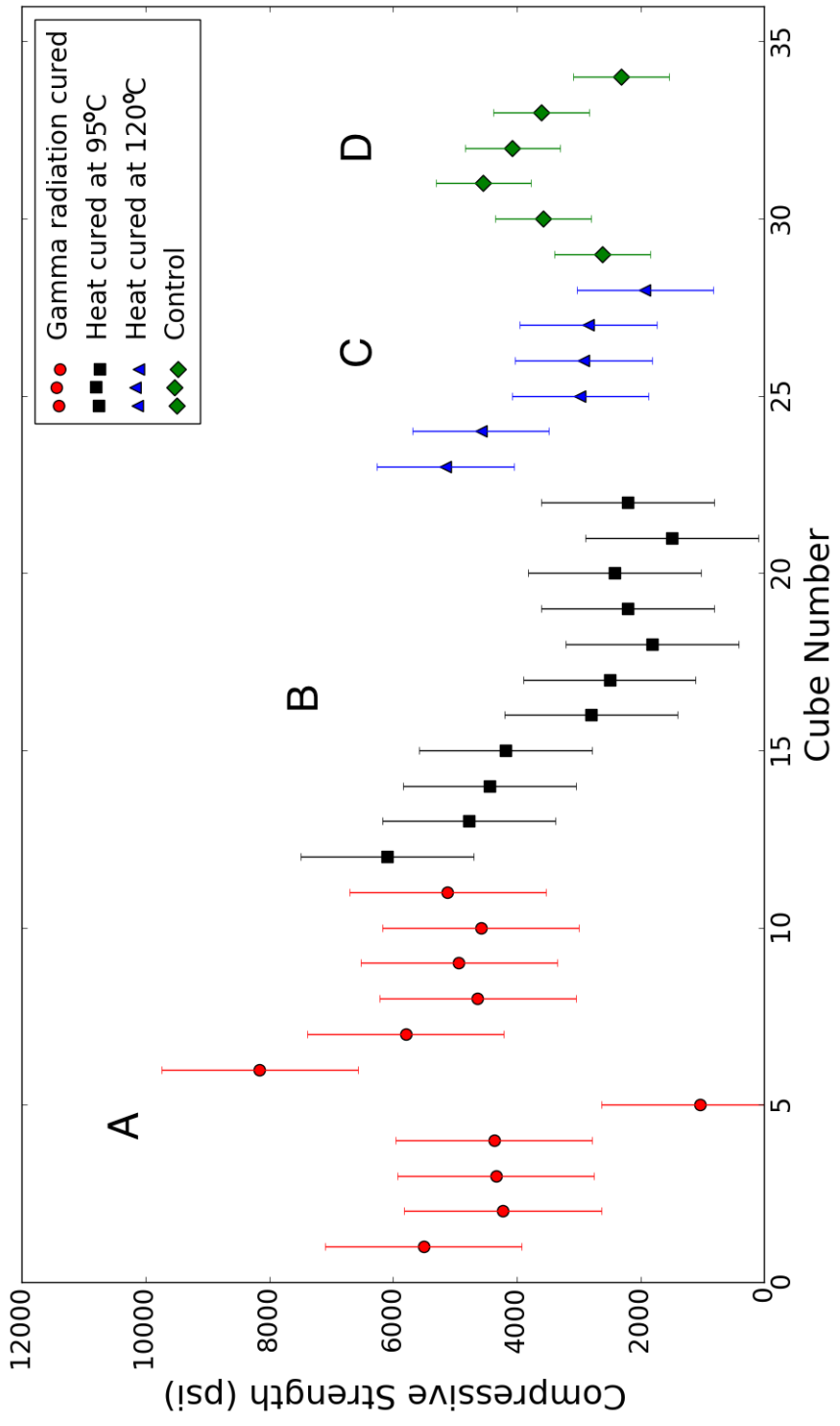

Fig. 2.11: Compressive strength of gamma cured, heat cured cubes at 95°C, heat cured cubes at 120°C, and control concrete cubes. The control cubes were cured without any heat or gamma ray exposure.

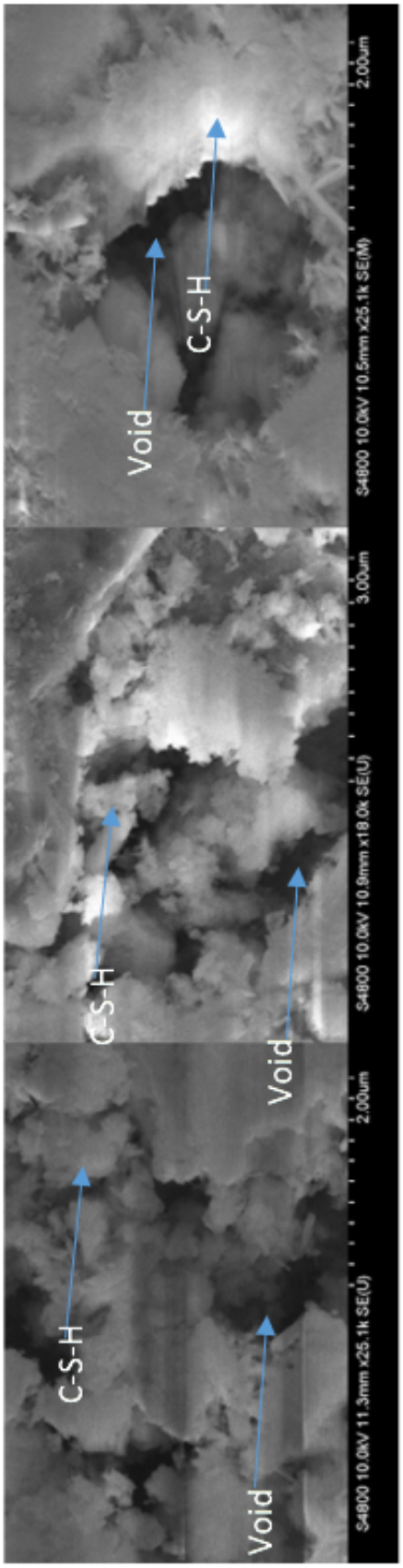

Fig. 2.12: SEM images of (a) gamma cured concrete (cube 6 of batch A in Fig. 2.11), (b) heat cured at 95°C (cube 1 of batch B shown in Fig. 2.11), and (c) heat cured at 120°C (cube 1 of batch C shown in Fig. 2.11). Each of these cubes has the highest compressive strength among the gamma cured ones, heat cured at 95°C, and heat cured at 120C as shown in Fig. 2.11.

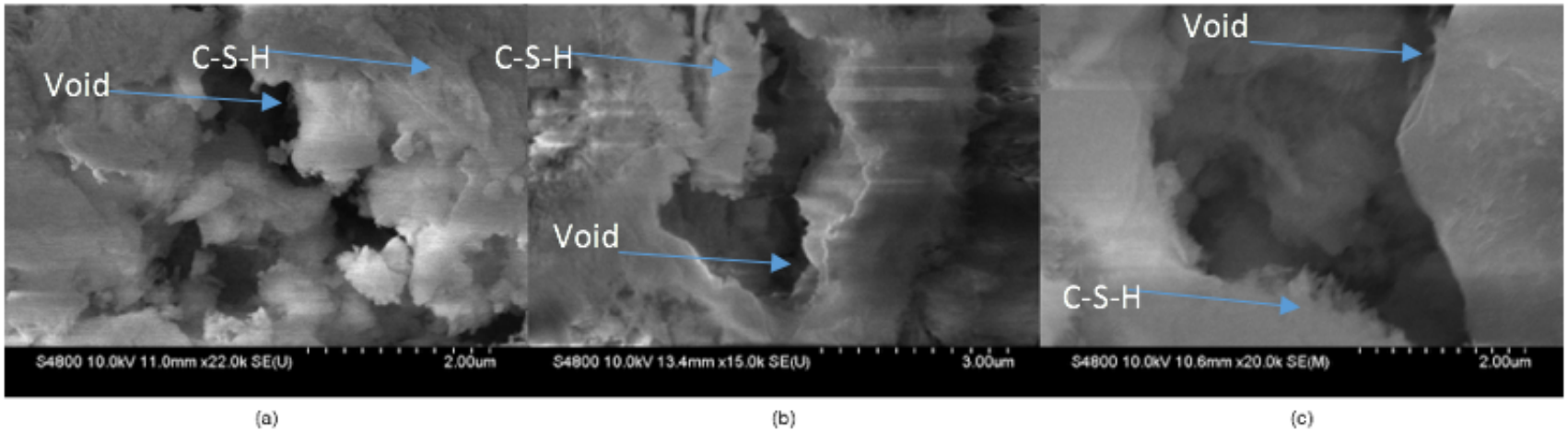

Fig. 2.13: SEM images of (a) gamma cured concrete (cube 5 of batch A in Fig. 2.11), (b) heat cured at 95°C (cube 10 of batch B in Fig. 2.11), and (c) heat cured at 120°C (cube 6 of batch C in Fig. 2.11). Each of these cubes has the lowest compressive strength among the gamma cured, heat cured at 95°C, and heat cured at 120°C as shown in Fig. 2.11.

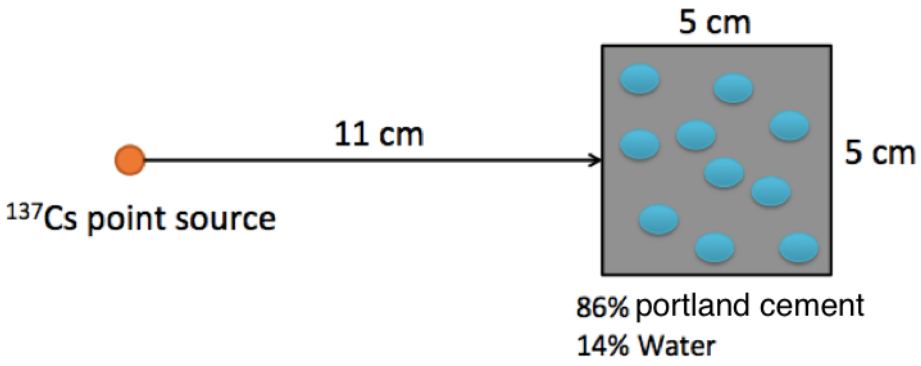

Fig. 2.14: Geant4 simulation geometry of gamma rays from a ^{137}Cs source interacting with concrete and leading the formation of free radicals.

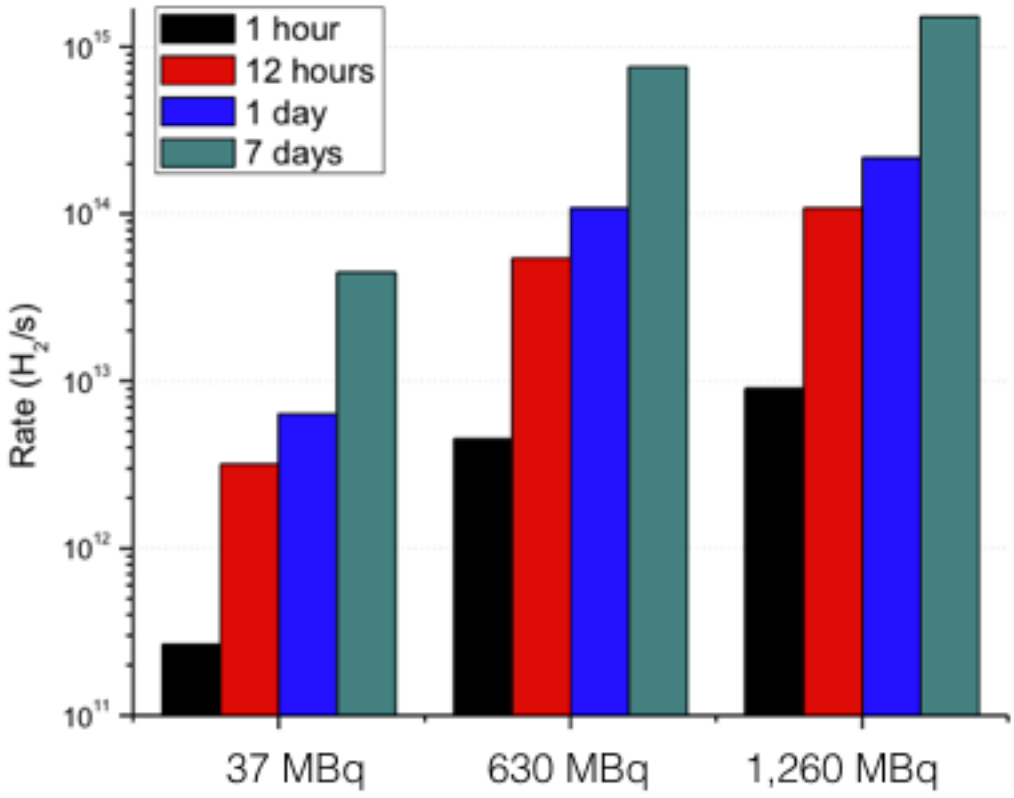

Fig. 2.15: Production of the H_2 radical within the micro pores of a 125 cm^3 sample of concrete in moles/s.

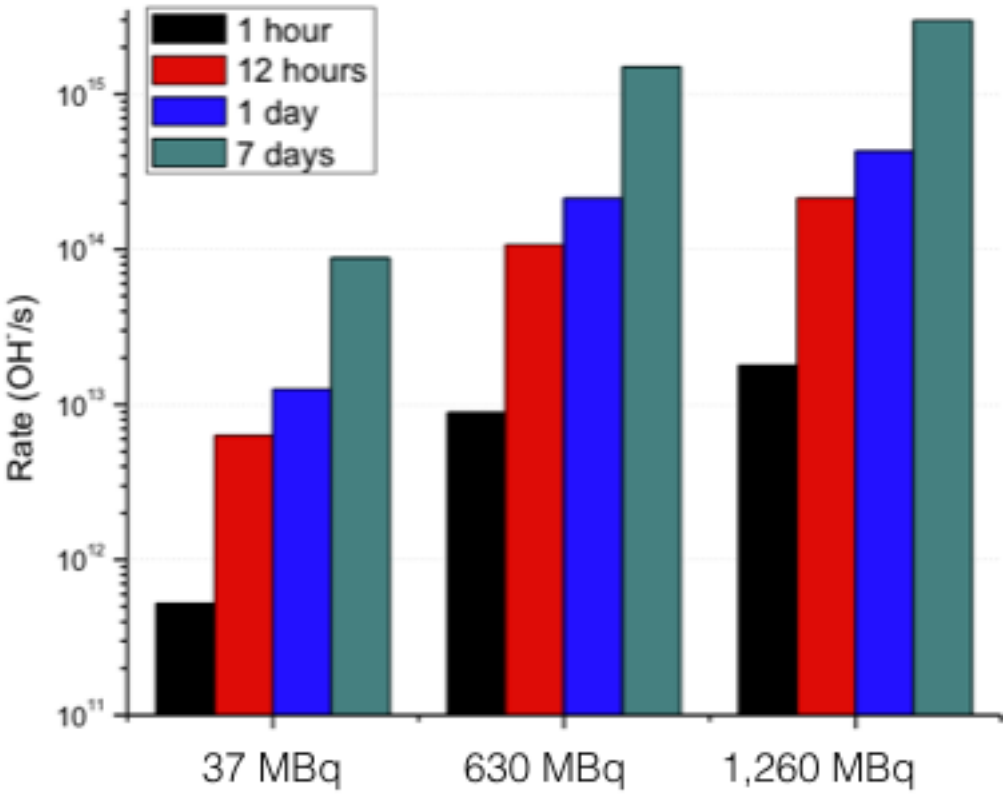

Fig. 2.16: Production of OH^- radical within the micro pores of a 125 cm^3 sample of concrete in moles/s.

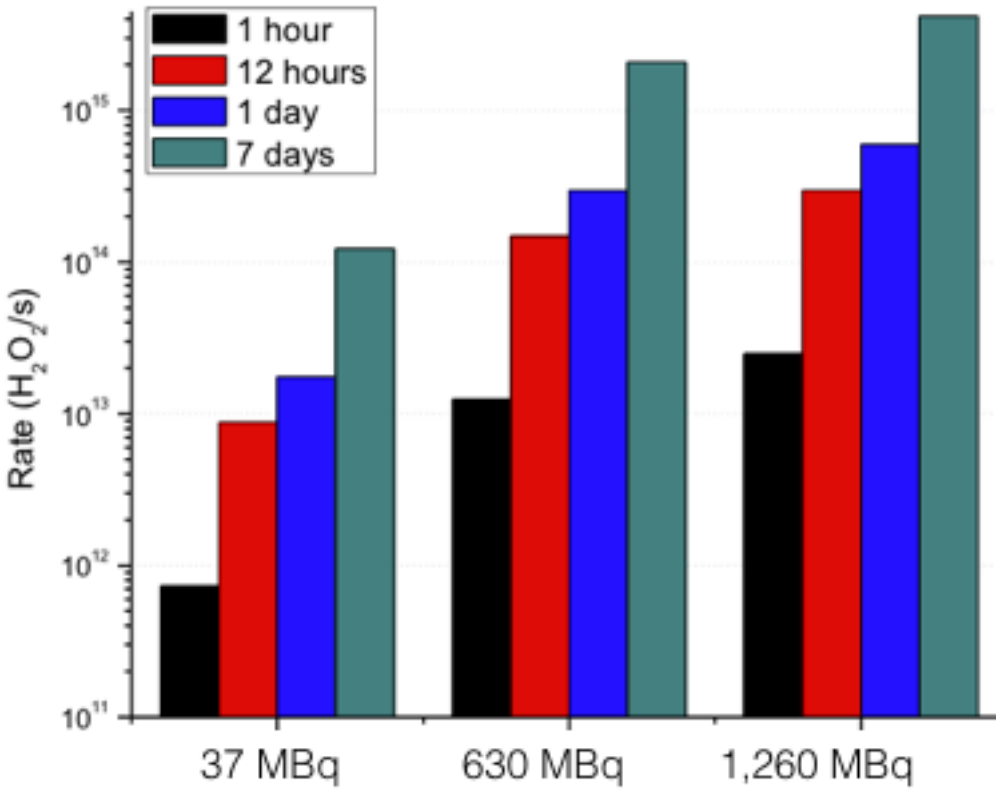

Fig. 2.17: Production of H_2O_2 radical within the micro pores of a 125 cm^3 sample of concrete in moles/s.

CHAPTER 3

COMPUTATIONAL AND EXPERIMENTAL ANALYSIS OF FUNDAMENTAL CHEMICAL PROCESSES DRIVEN BY LOW GAMMA DOSE RADIATION DURING EARLY STAGES OF CONCRETE CURING[1]

3.1 Abstract

High-dose gamma radiation is well documented as a mechanism that damages concrete and decreases its compressive strength. We have shown in our previous study that concrete exposed to low-dose gamma radiation during the first seven days of curing can increase its compressive strength by an average of 24%. Therefore, we now study the effects that low-dose gamma radiation has on concrete for 14 and 28 days of exposure to determine at what point the maximum benefit for gamma curing is achieved. Concrete cubes that are exposed to low-dose gamma radiation for 14 days show an increase in strength of 76% while if exposed for 28 days, gamma curing has no benefit. Due to inconsistencies in fine aggregate sourcing, compressive strength of 14 and 28 days cured cubes is shown to be less than cubes cured for seven days due to inconsistences in fine aggregate sourcing. Using SEM imaging, the microstructure is observed to see if any gamma heating is occurring. The microstructures between gamma cured and conventionally cured showed no differences, ensuring low-dose gamma radiation improves compressive strength without damaging its microstructure. Molecular dynamics modeling is used to determine the mechanism whereby gamma curing affects compressive strength. Using the MOPAC code, alite and belite, compounds in cement, are analyzed with and without free radicals present. Jennite and Tobermorite, two of many C-S-H structures, are also modeled in the MOPAC code to calculate their reactivity between water and aggregate. The reactivity between alite, belite, water, and silicate is improved when free

[1] Steven Burnham, Quentin Faure, Jake Tuttle, Jean-Nicolas Dupre, Keith Prisbrey, and Tatjana Jevremovic, "Computational and Experimental Analysis of Fundamental Chemical Processes Driven by Low Gamma Dose Radiation During Early Stages of Concrete Curing", Submitted to *Nuclear Engineering and Technology*, February 17, 2017.

radicals are present. Tobermorite and Jennite also show improved reactivity between water and silicate when free radicals are present, which may offer better hydration and bonding, ultimately resulting in improved compressive strength.

3.2 Introduction

The damaging effects that long-term and high-dose radiation have on the physical properties of concrete are well known and well documented. High doses of gamma radiation exposure have been shown to cause shrinkage and expansion, ultimately leading to a reduction in compressive strength [28]. Such doses are on the order of 10^7-10^{11} Gy [19, 20]. When concrete is exposed to doses this high, the crystal lattice structure of different molecules important to structural properties may become distorted. Distortions may cause molecules that would otherwise be unreactive to become reactive with the environment, resulting in degradation effects such as Alkali Silica Reactions (ASR) [19]. The damage from ASR results in a swelling of aggregates, placing internal stress on concrete that results in cracking and ultimately a loss of compressive strength or internal corrosion [6]. As gamma rays interact with concrete, they deposit their energy, resulting in the generation of heat. With high-dose gamma radiation, the energy transfer is sufficiently high to cause a noticeable rise in temperature as high as 250C, with damage occurring at temperatures as low as 95ºC [21].

It has been shown [3, 4] that low-dose gamma radiation can improve concrete compressive strength when concrete is exposed during the early stages of curing. The early stage of curing is defined as the first seven days out of 28 total days of curing time. When concrete that is exposed to gamma radiation during these first seven days is tested for compressive strength, an improvement of 24% is shown versus concrete that was cured conventionally [3, 4]. The effects of gamma curing on concrete up to the full 28 days of curing, as well as the mechanism whereby gamma radiation improves compressive strength, are further explored in this paper.

3.3 Chemistry and Hydration of Cement

Cement, the primary binding ingredient in concrete, is primarily composed of calcium silicates. As such, the materials used in the production of cement must be high in concentration of calcium and silica. Materials that are naturally occurring such as limestone are common sources of obtaining calcium while quartz or clay can be a natural source of the silica. The raw ingredients are crushed, mixed, and subjected to high temperatures to form cement. The result of the raw ingredients combining while under heat in excess of 1000ºC is the formation of a number of oxides and compounds known as clinker. The clinker is pulverized to a particle size of 10-15 μm, a form where it can then be mixed with other ingredients to form concrete. Table 3.1 summarizes all the oxides and compounds found in cement, the primary and most important being CaO and SiO_2 [7].

The oxides CaO and SiO_2 combine to form the two most important compounds in cement, tricalcium silicate ($3CaO \cdot SiO_2$) and dicalcium silicate ($2CaO \cdot SiO_2$), known as alite and belite, respectively [6]. The compound alite can account for 50-70% [41] of the composition of portland cement and is the most important constituent in portland cement. Its importance is a result of both the large amount in cement as well as its quick reaction with water, contributing to early-stage (seven days or less) strength. Belite will amount to 15-40% [41] of portland cement and reacts slowly with water. Belite contributes less to early-stage strength of concrete than alite due to its slow reaction but does contribute to the late-stage (28 days or more) strength. In general, the silicates account for approximately 75% of portland cement while the aluminates account for the other 25% [7]. When alite and belite are formed, their crystal structures become modified from contaminates in the raw materials such as limestone and quartz during production of clinker at high temperature. Contaminates such as iron, magnesium, and aluminum can change the reactivity of alite and belite with water [7].

When cement is produced, it is anhydrous. Mixing with aggregates in its anhydrous form does not allow for cement to bind with the aggregate and form concrete. When cement is mixed with water, the process of hydration occurs or the process whereby anhydrous cement reacts with water, forming products of hydration. The amount of water mixed with cement is known as the water to cement (w/c) ratio. When cement is mixed at a w/c ratio between approximately 0.3 and 0.6, a cement paste is formed [41]. The paste hardens in a process known as setting, a loss of its plastic state. Due to the variety of compounds present in portland cement, a variety of reactions take place when it is mixed with water. The aluminate compounds are the first to react with water and undergo hydration at a faster rate than the silicates. The loss of plasticity in cement paste is primarily due to the hydration of the aluminates. The silicates, which react at a slower rate the aluminates, are responsible for the solidification of portland cement. The silicates also have a much greater influence on the compressive strength properties.

Hydration of the silicates produces a variety of calcium-silica-hydrates and is abbreviated C-S-H. The dashes indicate the complexity and variety of C-S-H products that can be formed. The complexity is a result of the degree of hydration of the silicates that can occur and is dependent on the w/c ratio. The approximate chemical reaction for complete hydration of alite and belite is shown in Equations 3.1 and 3.2, respectively [6]:

$$6CaO \cdot SiO_2 + 6H_2O \rightarrow 3CaO \cdot SiO_2 \cdot 3H_2O + 3CaO \cdot H_2O \tag{3.1}$$

$$4CaO \cdot SiO_2 + 4H_2O \rightarrow 3CaO \cdot SiO_2 \cdot 3H_2O + CaO \cdot H_2O \tag{3.2}$$

Based on the stoichiometry of the above reactions, it is evident that belite (Eq. 3.2) produces a higher percentage of C-S-H and a lower percentage of calcium hydroxide. A cement with higher

concentrations of belite will yield higher strength compared to a cement with a higher concentration of alite. The slow reaction of belite compared to alite means that although the ultimate strength of a belite-rich cement has a higher ultimate compressive strength, it is much slower in achieving that strength in comparison to normal cements with a primary composition of alite. The calcium hydroxide has long-term effects on durability of concrete. An increased amount of calcium hydroxide will make concrete more susceptible to acid and sulfate attacks. Despite the possible benefits of increased amounts of belite in portland cement, alite remains the dominant compound due to its ability to quickly gain strength.

Since hydration of alite and belite is imperfect, Equations 3.1 and 3.2 are not representative of all the reactions that are occurring when portland cement undergoes hydration. A general formula of $CaO_x \cdot SiO_2 \cdot H_2O_y$ is used to represent the complex stoichiometry that can occur during hydration where x and y vary over a wide range [7]. The variations in stoichiometry are a result of partial or incomplete hydration of alite and belite. Factors that can affect the degree of hydration is the w/c ratio used, poor mixing, external humidity, as well as the fineness of the cement grains. The average ratio between CaO and SiO_2 ranges between about 1.4 – 2.0.

3.3.1 Mechanism of Hydration

The process of hydration can be divided into four phases: Initial mixing, dormant period, acceleration stage, and the post-acceleration period [6].

The initial phase is when cement first contacts water. The oxides and compounds immediately move into solution by dissolving. C-S-H also begins to form from the hydration of alite. The belite will contribute very little during this phase to C-S-H production.

The dormant phase starts a few hours after the initial phase begins. It is aptly named the dormant phase as hydration slows down significantly. Hydration of alite and other compounds progresses but at a much slower rate than during initial mixing.

The acceleration phase also begins to occur several hours after the initial phase (approximately 3-12 hours). Hydration of alite accelerates. The belite also begins to undergo hydration but still at a much slower rate than the alite. Calcium hydroxide also forms at a more rapid rate. This is exhibited in the stoichiometry of the reaction between alite and water where calcium hydroxide is formed at a rate of three to one compared to the reaction between belite and water. The potential drawbacks of higher calcium hydroxide from hydration can be mitigated by introducing other ingredients into concrete such as fly ash or pozzolans that readily react with the excess calcium hydroxide, thereby mitigating its damaging effects. This reaction is shown in Equation 3.3.

$$\text{Pozzolan} + CaO \cdot H_2O + H_2O \rightarrow C - S - H \tag{3.3}$$

Following the acceleration phase, the rate at which hydration occurs begins to decrease. The reason for the decline in hydration is in large part due to the decrease in the amount of unreacted alite. Hydration still does occur, however, thanks to the presence of belite in cement. The hydration of belite will increase over time but never at the same rate at which alite undergoes hydration. Calcium hydroxide will form at a slower rate as well thanks to the stoichiometry as previously stated in the acceleration phase. Hydration of cement occurs so long as there are unreacted cement particles and water molecules. Concrete mixtures that contain low w/c ratios will undergo a partial or incomplete hydration due to insufficient water to complete the process. The fineness of cement particles may also influence the post-acceleration phase. A fine cement will disperse more readily and allow a more complete reaction. Coarse cement particles are more likely to persist indefinitely due to their inability to disperse where unreacted water may exist.

3.3.2 Cement Hydration and Its Relation to Gamma Curing

In freshly mixed concrete, a high amount of free water is present. Exposure to gamma radiation results in an interaction between water molecules and gamma-rays, resulting in radiolysis occurring. Radiolysis is the process whereby free radicals are formed when one of several different interactions can take place, dependent on photon energy, such as photoelectric effect or Compton scattering. Radiolysis is described as follows:

$$H_2O \xrightarrow{\text{ionizing radiation}} e_{aq}^{-},\ HO,\ H,\ HO_2,\ H_3O,\ H_3O^{+},\ OH^{-},\ H_2O_2,\ H_2 \tag{3.4}$$

Free radicals may interact with themselves, forming water once again, or they may also interact with the aqueous solution of cement and water. The breakdown of water and formation of free radicals from radiolysis may allow constituents within cement to more freely interact. It follows then that by using the principles of radiolysis from gamma ray interactions with water, the curing phase of concrete may be enhanced by exposure to low-dose gamma radiation.

3.4 Examining the Effects of Gamma Radiation on Concrete Cured to 28-Days

As discussed in Section 3.1, gamma radiation may enhance the curing phase of concrete when a high amount of free water is present. It has been shown [3] that compressive strength of gamma cured concrete cubes is increased by an average of 24% in the first seven days of curing. The process of mixing, curing, and strength testing from our previous study [3] is briefly described as follows:

- A mix design of 0.4 water to cement (w/c) ratio with only fine aggregates (sand) mixed in a 2.75 sand to cement (s/c) ratio is used for all concrete mixtures.
- Concrete cubes 125 cm^3 are cast for each batch of concrete for compressive strength testing.

- To ensure consistency between batches of concrete, the procedure for mixing the concrete cubes outlined in ASTM Standard C192/192M – Making and Curing Concrete Test Specimens in the Laboratory [31] is adhered to with the exception of concrete cubes being demolded five hours after casting. This is done so that the concrete cubes may be exposed to gamma radiation at the very earliest stages of curing when a maximum available amount of free water is present for radiolysis to occur.
- Half of all concrete cubes are cured using a 630 MBq ^{137}Cs while the other half are conventionally cured for seven, 14, or 28 days. The absorbed dose from gamma curing is determined experimentally for seven days and computationally for seven, 14, and 28 days [3]. The average experimentally determined dose is 69.1 cGy while the computationally determined dose using MCNP6 is 66.0 cGy for seven days of exposure, 1.32 Gy for 14 days of exposure, and 2.64 Gy for 28 days of exposure.
- Following curing, cubes are tested for compressive strength in accordance with ASTM standard C109 – Standard Test Method for Compressive Strength of Hydraulic Cement Mortars [35].

Using the above procedure, it was shown in our previous study [3] that gamma cured concrete has a seven-day compressive strength range of 48 – 73 MPa with an average of 61 MPa while conventionally cured concrete cubes have a compressive strength range of 24 – 65 MPa with an average of 49 MPa. When concrete cubes are cured for 14 days using the same methodology, the compressive strength of the gamma cured cubes is found to be 29 – 59 MPa with an average of 45 MPa while the conventionally cured cubes are 25 MPa. The results of 14-day compressive strength testing are shown in Fig. 3.1. A statistical t-test is performed to compare the sameness of the data sets of gamma cured and conventionally cured cubes. A p-value is obtained, representing the probability that the two data sets are different, of 0.0004, indicating that the two data sets are different and that the gamma cured cubes have a statistically significant compressive strength that is higher than the conventionally cured cubes.

Using the same procedure, compressive strength is also tested after 28-days of curing. The 28-day compressive strength of gamma cured cubes is between 25 – 58 MPa with an average of 50 MPa while the conventionally cured cubes are between 26 – 68 MPa with an average of 51 MPa, as shown in Fig. 3.2. The same t-test is performed to compare the data sets of 28-days cured concrete cubes. A p-value of 0.82 is obtained, representing an 82% probability that the two data sets are statically the same. It follows therefore that the benefits of gamma curing exist during the earliest stages of curing. The cubes tested at seven days exhibited an increase in compressive strength of 24%. The cubes tested at 14 days exhibited a compressive strength increase of 76%. After 28 days of exposure,

the benefits of gamma curing are nonexistent. A summary of the average compressive strength of seven, 14, and 28 day cured cubes is shown in Table 3.2. The average strength between 14 and 28 days gamma cured and conventionally cured cubes increases as is expected with increasing curing time. The average strength, however, decreases from seven to 14 days curing time for both gamma cured and conventionally cured cubes. This trend is attributed to changes in the fine aggregate source used for all concrete mixes. The cubes cured for seven days were tested several months before experiments for 14 and 28 days were performed. While the mix design was tightly controlled to be the same for all concrete mixtures, the fine aggregate source was not homogenous, resulting in 14 and 28 days cured cubes with lower strength than the cubes cured for seven days.

3.5 Examination of the Microstructure of Gamma Cured and Conventionally Cured Concrete Cubes Using Scanning Electron Microscope (SEM)

As described in Section 3.1, it is well understood that high-dose gamma radiation can structurally damage concrete. These effects are exhibited in displacement of the crystal structure of molecules in concrete as well as from gamma heating. Visually, these defects manifest themselves as cracks, voids, and low density, all visible at the microscopic level using SEM [42].

Using SEM (Hitachi S-4800 SEM in the Crus Advanced Materials Technology Center at the University of Utah), the microstructure of seven, 14, and 28 days cured concrete cubes, both gamma and conventionally cured, are examined to determine if any radiation damage is occurring. While the concrete cured at seven and 14 days with gamma radiation exhibited higher compressive strength, structural defects may be possible that could lead to a decrease in durability, affecting the long-term structural integrity of the concrete. In Fig. 3.3, the microstructure of concrete cubes cured for seven days is shown for both gamma cured and conventionally cured. From the images, it is apparent that both the gamma cured and conventionally cured cubes exhibit well-developed C-S-H as well as a low void ratio. The conventionally cured cube has a larger void than the gamma cured cube.

At the microscopic level, damage occurring from heat exposure up to 600ºC is easily visible at a resolution of 1-5 m [42]. Dehydration of C-S-H is also visible at these resolutions. The resolution of the SEM images in Figures 3.3 and 3.4 is between 2-4 m, a resolution where structural damage from gamma heating or dehydration of C-S-H due to radiolysis is visible. The similarities of the gamma cured and conventionally cured cubes is indicative of two things: no gamma heating is occurring to a level that the microstructure is damaged and dehydration of C-S-H is not occurring from radiolysis. The SEM images show that the long-term durability of concrete is not compromised when exposed to low doses of radiation for short periods of time.

3.6 Computational Model of Cement Hydration Chemical Process

To determine the effects gamma curing has at the atomistic level, the reactions taking place between free radicals and cement, as described in Section 3.3, are studied using Molecular Dynamics (MD) simulations. The use of MD software allows for the observation of the interactions taking place between different molecules present in the cement hydration process. These interactions are not visible using experimental processes such as SEM.

Using frontier molecular orbital theory [43, 44], the energies of the Highest Occupied Molecular Orbital (HOMO) and Lowest Unoccupied Molecular Orbital (LUMO) are determined using the semi-empirical MD package MOPAC (Molecular Orbital PACkage) 2016 [45]. To determine reactivity between two molecules, the absolute value of the energy gap between the HOMO and LUMO and the LUMO and HOMO of the two molecules is calculated as shown in Equations 3.5 and 3.6 to determine the reactivity. The lower of these two values is the most probabilistic reaction to take place. In other words, as the gap between the HOMO and LUMO or LUMO and HOMO approaches zero, the reactivity between the two molecules increases.

$$\mid \text{HOMO} - \text{LUMO} \mid = \text{Reactivity}\,(\text{eV}) \tag{3.5}$$

$$\mid \text{LUMO} - \text{HOMO} \mid = \text{Reactivity}\,(\text{eV}) \tag{3.6}$$

The crystal structures of the compounds modeled in MOPAC are obtained from the American Mineralogist Crystal Structure Database [46] and are as follows:

- Alite ($3CaO \cdot SiO_2$)
- Belite ($2CaO \cdot SiO_2$)
- Tobermorite ($Ca_5Si_6O_{16}(OH)_2 \cdot 4H_2O$)
- Jennite ($Ca_9Si_6O_{18}(OH)_6 \cdot 8H_2O$)
- Water (H_2O)
- Silicate (SiO_3)

The compounds are modeled in MOPAC to determine the HOMO and LUMO as follows:

1. Individual molecules of alite, belite, Tobermorite, Jennite, water, and silicate are simulated and their HOMO-LUMO values determined without any radiolysis products. Six simulations are run in total.
2. One H^+ molecule is introduced to the alite, belite, Tobermorite, and Jennite molecules and the simulation is run again. Additional H^+ molecules are introduced in increments of one with the simulation running again after each H^+ molecule is added up to a total of 10 H^+ molecules. In total, 40 simulations are run, 10 each for alite, belite, Tobermorite, and Jennite.

3. Step 2 is repeated for OH^- and H_3O^+ for each of the molecules, totaling 80 additional simulations.
4. Using Equations 3.5 and 3.6, the absolute value of the HOMO-LUMO and LUMO-HOMO is calculated for the alite, belite, Tobermorite, and Jennite modeled in Step 1 with water and silicate. Comparison between the individual molecules with water and silicate determines a baseline for reactivity when no radiolysis products are present, i.e, no gamma curing is occurring.
5. Using Equations 3.5 and 3.6, the absolute values of HOMO-LUMO and LUMO-HOMO is then calculated for alite, belite, Tobermorite, and Jennite when radiolysis products are present or those modeled in Steps 2 and 3. The lowest value of either HOMO-LUMO or LUMO-HOMO is determined to be the reactivity.

Using data from Table 3.3, an example of how the reactivity is calculated is shown below.

$$\mid \text{HOMO} - \text{LUMO} \mid = \mid -11.67 + 2.11 \mid = 9.56\text{eV} \tag{3.7}$$

$$\mid \text{LUMO} - \text{HOMO} \mid = \mid 3.77 + 3.17 \mid = 6.94\text{eV} \tag{3.8}$$

In the above example, the LUMO-HOMO yields the lowest number and is therefore considered to be the reactivity between water and alite. The reactivity of alite, belite, Tobermorite, and Jennite with water and silicate when free radicals are introduced is summarized in Figs 3.5 – 3.8.

In Fig. 3.5, the reactivity of alite and belite with water when free radicals are introduced is shown. As stated in Section 3.2, alite contributes to the early-stage strength of concrete as it reacts rapidly with water to form C-S-H, whereas belite contributes to later stage strength by reacting more slowly with water to form C-S-H. This is evident when comparing the baseline reactivates between alite (Fig. 3.5 top) and belite (Fig. 3.5 bottom) where alite's baseline reactivity of 6.94 eV is lower than belite's base reactivity of 8.43 eV. The baseline reactivity is defined as the reactivity of one molecule of either alite, belite, Jennite, or Tobermorite with either water or silica when no free radicals are present. When H_3O^+ and H^+ are present, the reactivity of alite with water increases in most instances. One exception is when one H^+ molecule is present, the reactivity between alite and water is improved. When OH^- is present, the reactivity between alite and water increases initially, but in most instances, it is improved. The reactivity energy drops from a baseline of 6.94 eV to as low as 5.20 eV when 10 hydroxides are present.

The reactivity of belite with water is greatly improved in most instances when free radicals are present. Two exceptions are when six H^+ molecules and nine OH^- molecules are present, the reactivity energy increases substantially. The addition of these free radicals causes a large gap in the HOMO and LUMO energies between belite and water.

Figure 3.6 shows the reactivity of alite and belite with fine aggregate, approximated as silicate, when free radicals are present. Alite has a baseline reactivity with silicate of 0.81 eV. When OH^- is introduced, the reactivity energy steadily increases, decreasing the overall favorability of a reaction between alite and silicate. The reaction when H^+ is present initially spikes when one H^+ molecule is present but maintains a similar reactivity energy for 2-10 H^+ molecules. The reactivity of alite with silicate is similar for H_3O^+ as it is for H^+.

Belite oscillates up and down from the baseline reactivity energy of 1.91 eV. When odd numbers of H_3O^+ are present, the reaction becomes less favorable between belite and silicate. When an odd number of OH^- is present, the reaction becomes more favorable. The reactivity of H^+ remains relatively constant with the baseline energy.

As stated in Section 3.3, when alite and belite react with water, C-S-H is formed. The C-S-H is what holds aggregate together in concrete. It is therefore expected that if gamma curing is improving compressive strength, it is improving the reactivity of alite and belite with water and not with silicate.

In Fig. 3.7, the reactivity of Jennite (top) and Tobermorite (bottom) and water are shown. It is apparent that the introduction of H^+, OH^-, H_3O^+ improves their reactivity with water in every instance. The addition of OH^- offers the greatest improvement in reactivity with Jennite's reactivity improving from a baseline of 8.90 eV to 3.48 eV when six OH^- molecules are present. When seven OH^- molecules are present for Tobermorite, the reactivity improves from a baseline energy of 10.28 eV to 5.22 eV. Both Jennite and Tobermorite have undergone hydration and formed C-S-H. As stated in Section 3.2, the structure of C-S-H is highly amorphous. One difference between Jennite and Tobermorite is Jennite is bonded with four water molecules while Tobermorite is bonded with eight molecules. The improved reactivity between Jennite and Tobermorite with water when free radicals are present may lead to C-S-H structures becoming more hydrated. Some of these more hydrated C-S-H structures may also have improved compressive strength over the less hydrated forms of C-S-H.

Figure 3.8 shows the reactivity of Jennite and Tobermorite when free radicals are present with fine aggregate, approximated as silicate. Jennite's reactivity follows a similar trend for the free radicals H^+, OH^-, and H_3O^+ in that an odd number of free radicals increases the reactivity energy above the baseline energy of 1.15 eV while an even number decreases the energy below the baseline. Tobermorite has improved reactivity with silicate in almost every instance when free radicals are present. With a baseline reactivity energy of 2.53 eV, the presence of two and four H_3O^+ molecules improves reactivity to a minimum energy of 0.03 eV.

The reaction between C-S-H structures and aggregate may be the most important in improving compressive strength. Because C-S-H is what bonds the aggregate together, it can often be where

modes of failure in concrete occur [7].

3.7 Conclusion

The damaging effects of gamma radiation on concrete at high doses are well studied and well documented. However, as we show in this paper, the low-dose gamma radiation to concrete during its curing shows an increase its compressive strength and does not produce any similar damage as with long-term exposure to gamma radiation. This seems to be on its own a very encouraging finding. According to our presented results, the exposure to gamma radiation during the first seven days of its curing increased compressive strength by 24%, if exposed to gamma radiation during the fist 14 days, the strength is improved for 76%, and if exposed for all 28 days of curing, no benefit in compressive strength compared to conventionally cured concrete is observed. Due to differences in fine aggregate sourcing, the compressive strength of cubes cured for 14 and 28 days was less than the cubes cured under the gamma field for seven days. While mix designs were tightly controlled, improvements in controlling fine aggregate sourcing is required; it will therefore allow for better comparison between these three different curing times, seven, 14, and 28 days. The SEM imaging is used to observe if any gamma heating occurs. It was found that there are no differences in the microstructure between gamma cured concrete and conventionally cured concrete, thus ensuring that the low-dose gamma radiation is indeed improving the strength without damaging its chemical structure.

The mechanism whereby gamma curing affects compressive strength is analyzed based on molecular dynamics modeling with the MOPAC code. Key compounds in cement, alite and belite, are analyzed by examining their reactivity with water and aggregate, because of gamma radiation exposure; it is analyzed with and without free radicals being present. Jennite and Tobermorite, two of many C-S-H structures, are also modeled to calculate the reactivity between water and aggregate. Reactivity between alite, belite, water, and silicate is improved in many instances when free radicals are present. An improvement in the reactivity between belite and water could be especially beneficial to concrete as it generally reacts slowly with water to form C-S-H. Tobermorite and Jennite reactivity is also improved with water and silicate when free radicals are present. Improved reactivity with water and silicate may allow C-S-H structures to become more hydrated and offer better bonding and as a result better compressive strength.

3.8 Acknowledgements

This research is supported by the Utah Nuclear Engineering Program, and the US NRC fellowship grant.

Table 3.1: Oxides and compounds present in cement

Oxide	Compound
CaO	$3CaO \cdot SiO_2$
SiO_2	$2CaO \cdot SiO_2$
Al_2O_3	$3CaO \cdot Al_2O_3$
Fe_2O_3	$4CaO \cdot Al_2O_3 \cdot Fe_2O_3$
MgO	$4CaO \cdot 3Al_2O_3 \cdot SO_3$
SO_3	$3CaO \cdot 2SiO_2 \cdot 3H_2O$
-	$CaSo_4 \cdot 2H_2O$

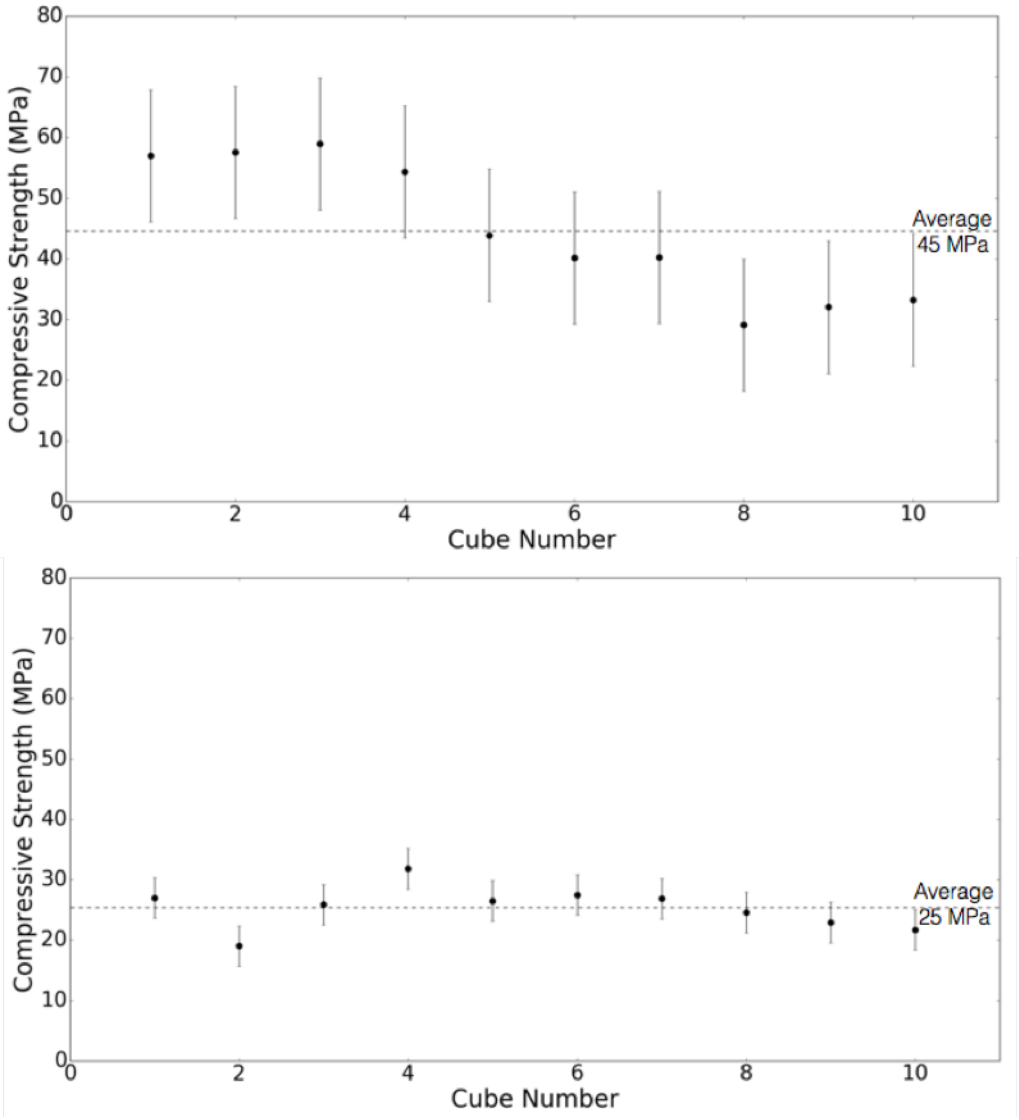

Fig. 3.1: Compressive strength gamma cured (top) and conventionally cured (bottom) concrete cubes after 14-days of curing following which compressive strength is tested.

Table 3.2: Comparison of the average compressive strength values for seven, 14, and 28 days gamma cured and conventionally cured concrete cubes

	Gamma Cured (MPa)	**Conventionally Cured (MPa)**
7 Days Average Compressive Strength	61	49
14 Days Average Compressive Strength	44	25
28 Days Average Compressive Strength	50	51

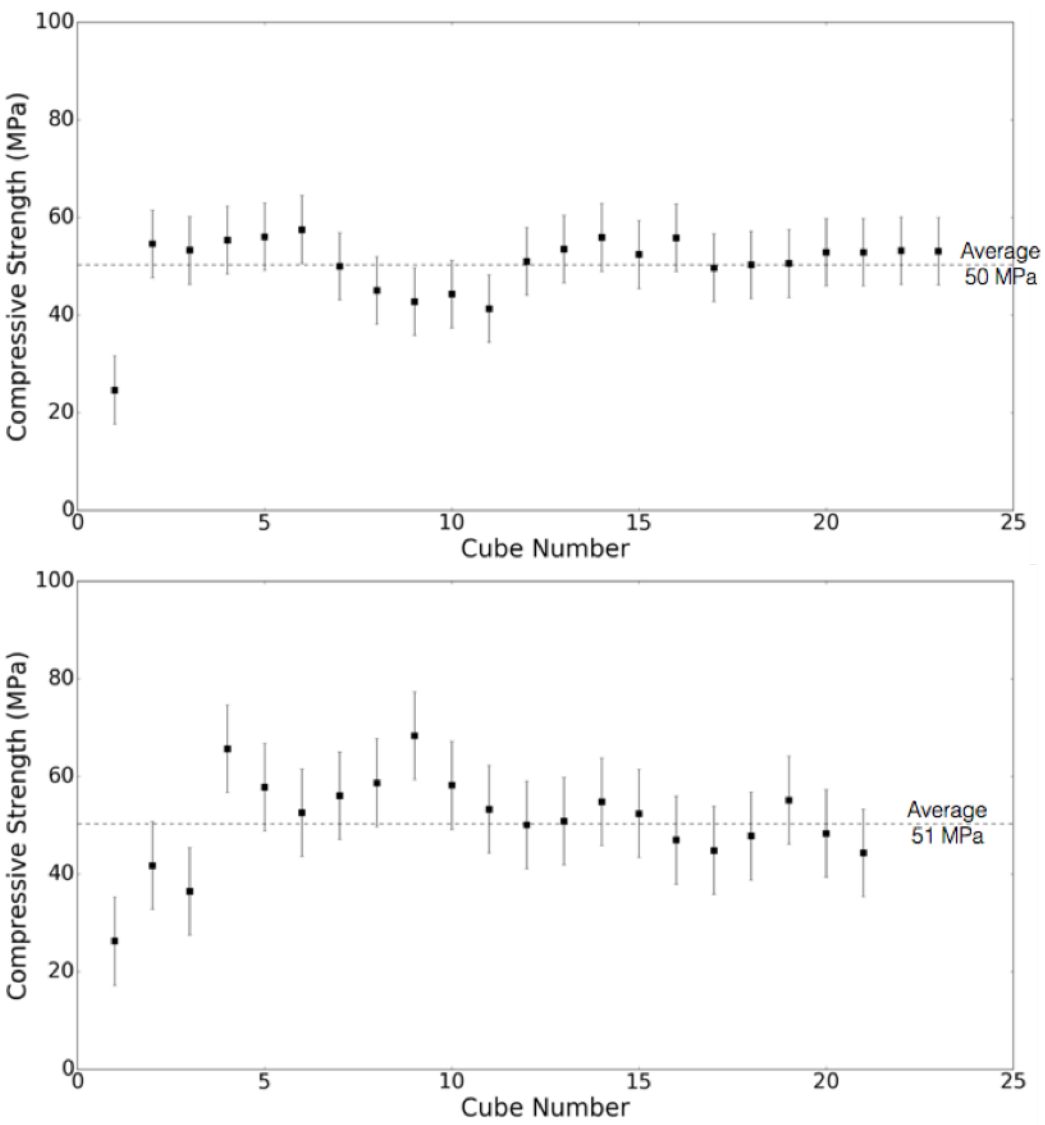

Fig. 3.2: Compressive strength gamma cured (top) and conventionally cured (bottom) concrete cubes after 28-days of curing following which compressive strength is tested.

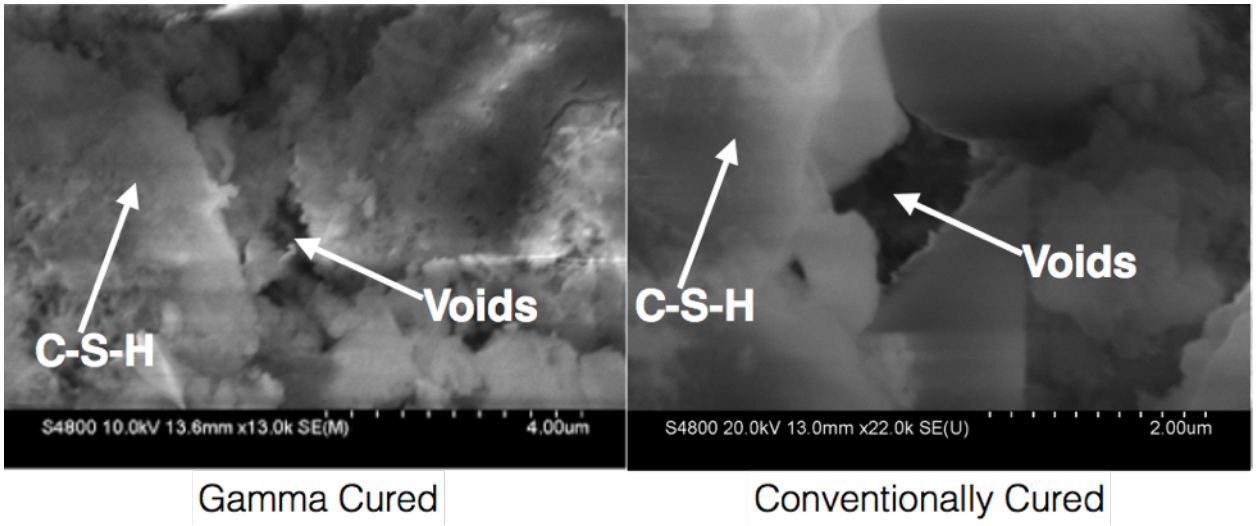

Fig. 3.3: SEM images of gamma cured (left) and conventionally cured (right) concrete cubes. Both cubes have well-developed C-S-H as well as a low void ratio.

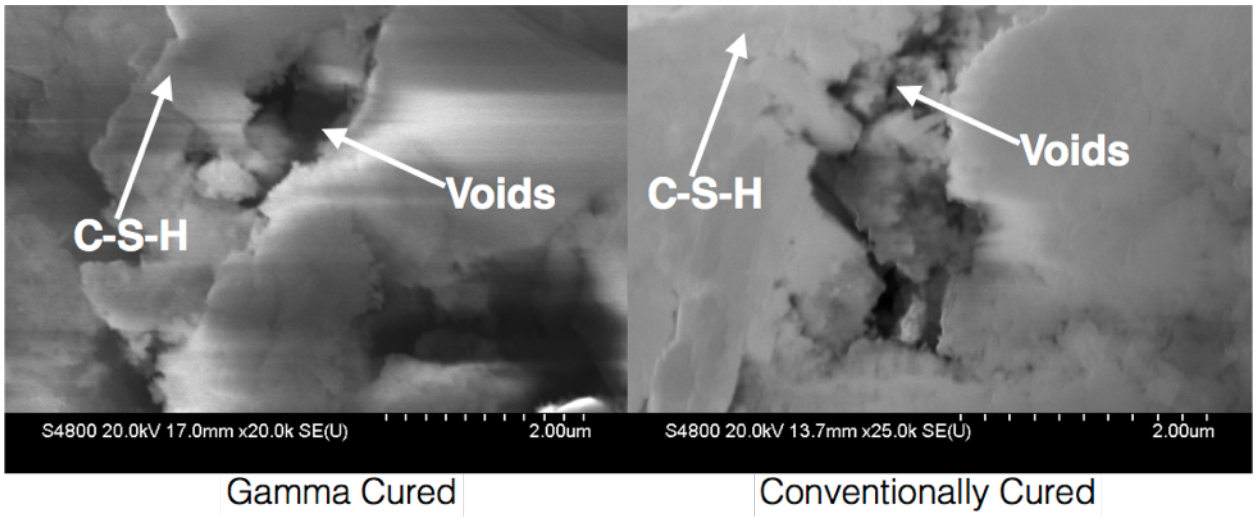

Fig. 3.4: SEM images of gamma cured (left) and conventionally cured (right) concrete cubes. The gamma cured and conventionally cured cube both have a high density of C-S-H with a low void ratio.

Table 3.3: The HOMO and LUMO values for water and alite as calculated using MOPAC

Molecule	**HOMO**	**LUMO**
Water	-11.67	3.77
Alite	-3.17	-2.11

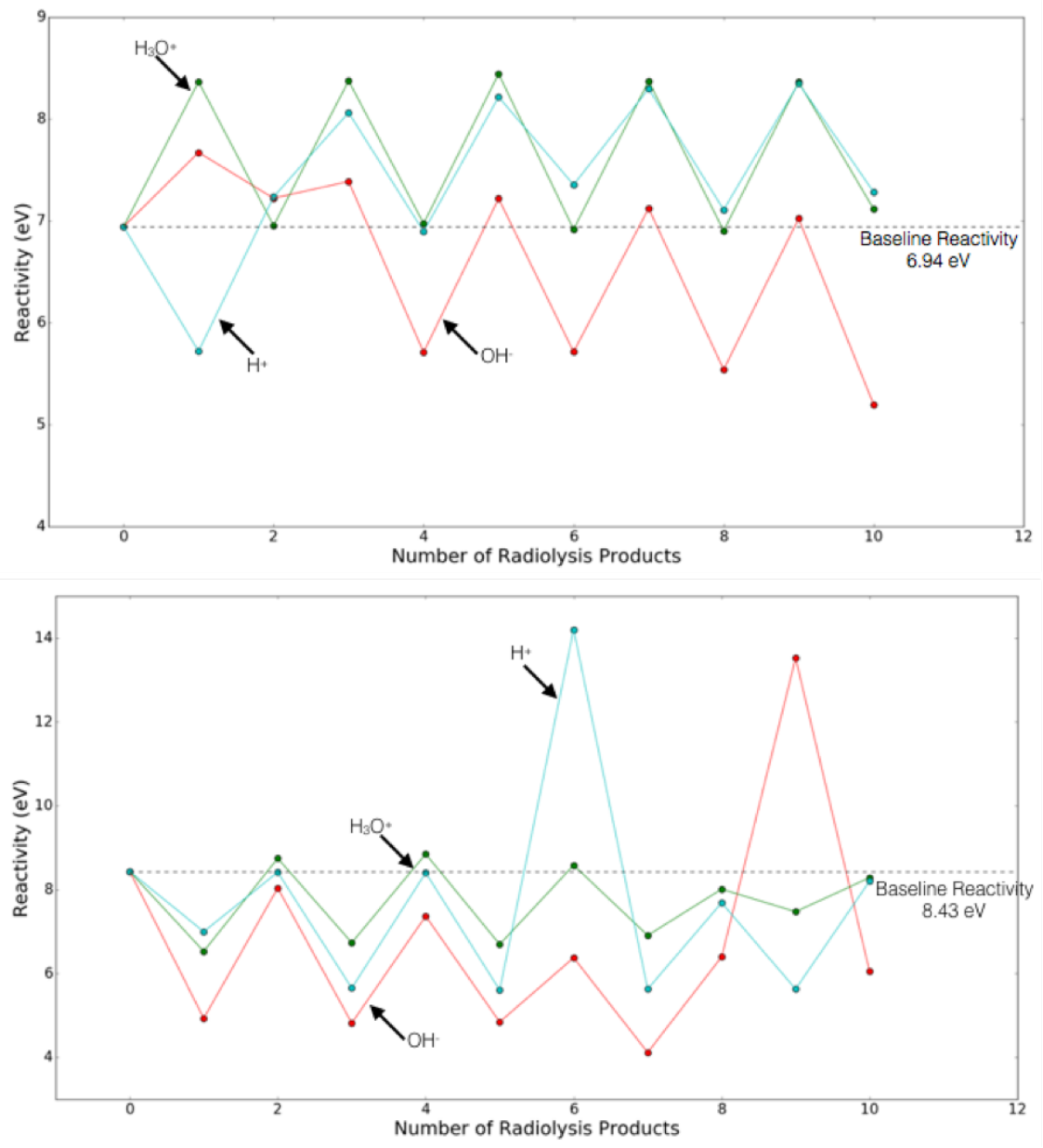

Fig. 3.5: Reactivity of alite (top) and belite (bottom) with water when the free radicals H^+, OH^-, and H_3O^+ are present. The baseline reactivity is defined as the reactivity of alite or belite with water when no free radicals are present. The lower the reactivity, the more favorable it is for the reaction to take place.

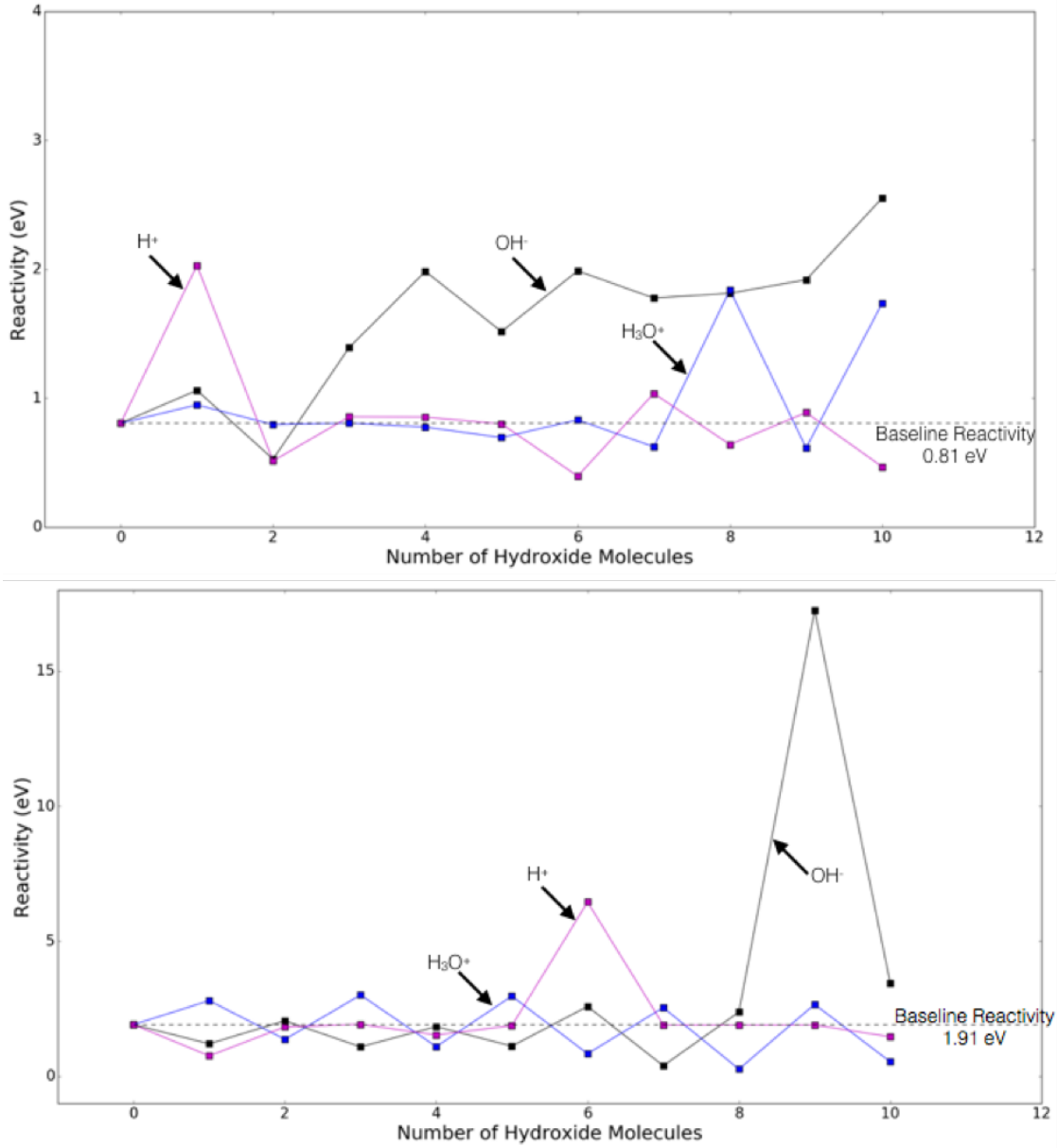

Fig. 3.6: Reactivity of alite (top) and belite (bottom) with silicate when the free radicals H^+, OH^-, and H_3O^+ are present. The baseline reactivity is defined as the reactivity of alite or belite with silicate when no free radicals are present. The lower the reactivity, the more favorable it is for the reaction to take place.

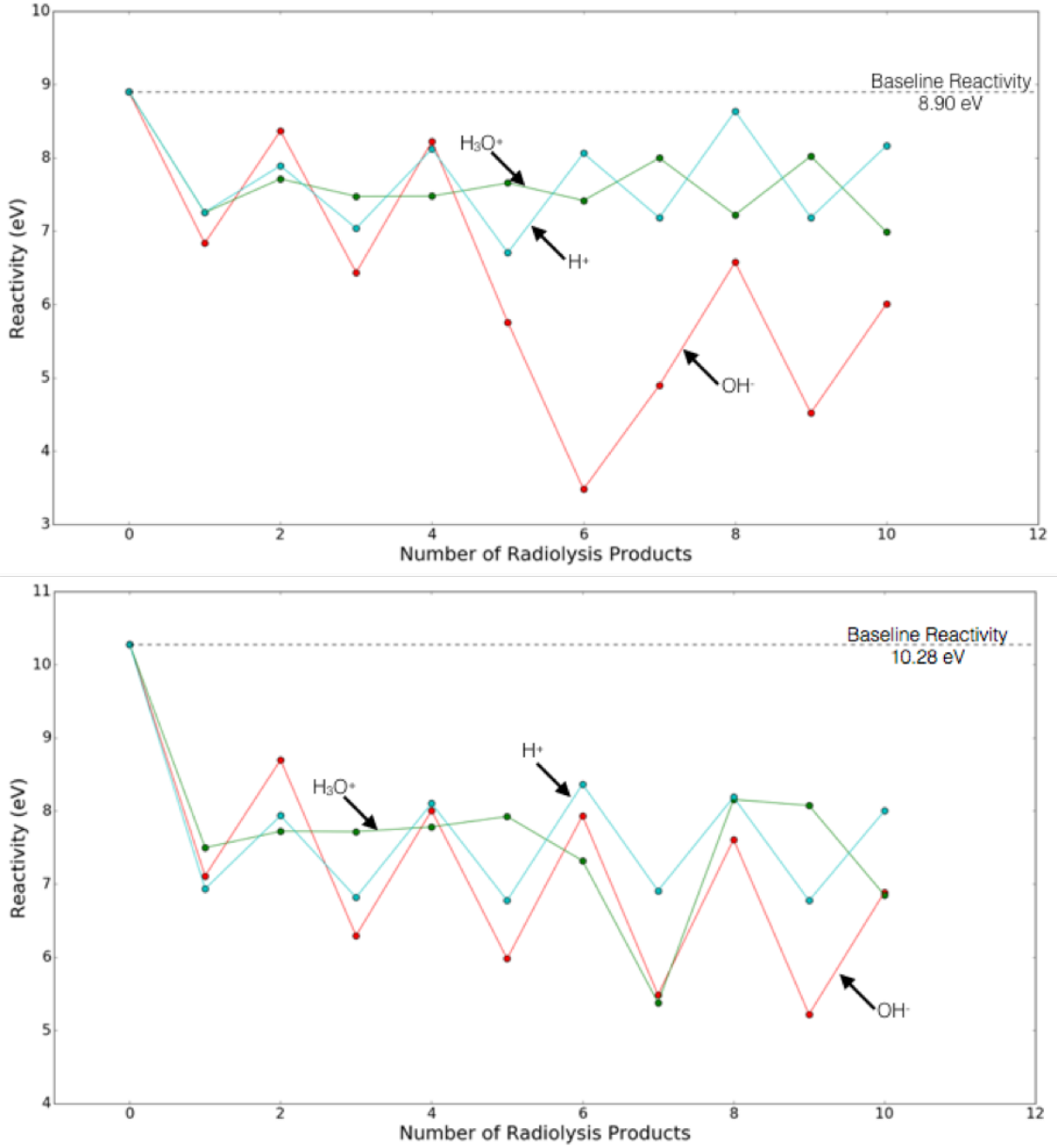

Fig. 3.7: Reactivity of C-S-H in the forms of Jennite (top) and Tobermorite (bottom) with water when the free radicals H^+, OH^-, and H_3O^+ are present. The baseline reactivity is defined as the reactivity of Jennite or Tobermorite with water when no free radicals are present. The lower the reactivity, the more favorable it is for the reaction to take place.

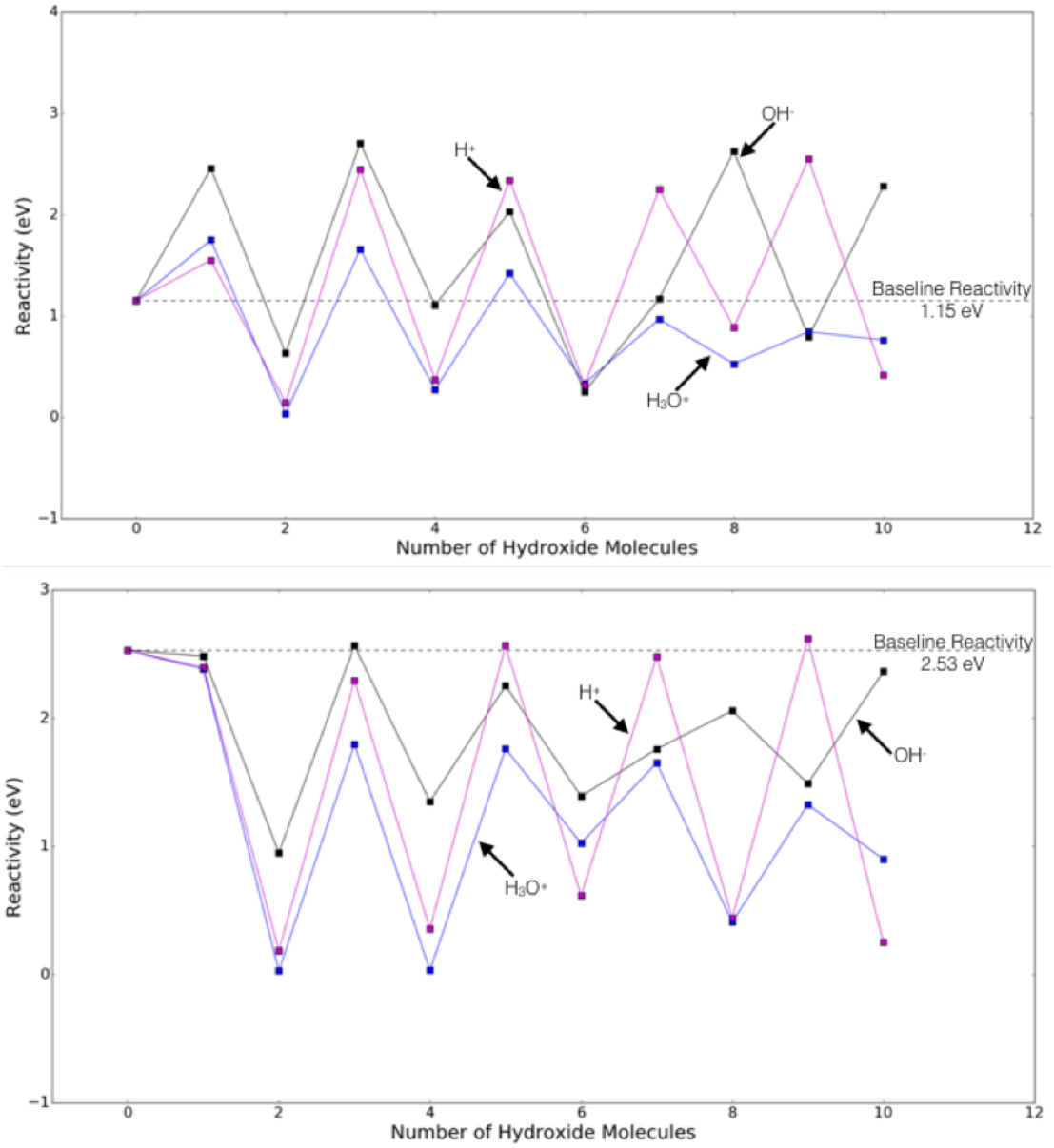

Fig. 3.8: Reactivity of C-S-H in the forms of Jennite (top) and Tobermorite (bottom) with silicate when the free radicals H^+, OH^-, H_3O^+ are present. The baseline reactivity is defined as the reactivity of Jennite or Tobermorite with silicate when no free radicals are present. The lower the reactivity, the more favorable it is for the reaction to take place.

CHAPTER 4

UNCERTAINTIES IN MEASURING TRACE AMOUNTS OF COBALT AND EUROPIUM WITH LOW FLUX NEUTRON ACTIVATION ANALYSIS[1]

4.1 Abstract

Neutron activation analysis (NAA) is widely used for identification of elements and their quantities even in trace amounts in the samples of almost any type. The challenges in detecting trace amounts of particular elements are often associated with the neutron flux produced at the research reactors. Low-flux NAA usually presents the biggest challenge when analyzing trace quantities of elements with a lower magnitude of radiative capture cross sections.

In this paper, we present the methodology and the quantified uncertainties associated with the detection of trace amounts of cobalt and europium, using concrete aggregates as an example. Recent growing interest is in improving structural concrete (increasing its strength but reducing its activation in the nuclear power plant (NPP) environments). Besides for buildings, structural concrete is also used as a biological shield in NPP that becomes radioactive after exposure to neutron flux. Due to radiative capture interactions, artificial radionuclides are generated to high enough concentrations that classify concrete as low-level radioactive waste at the time of the plant's decommissioning. Disposal of this concrete adds to the expense of NPP financing and its construction. Three radionuclides, ^{60}Co, ^{152}Eu, and ^{154}Eu, account for 99% of total residual radioactivity of NPP decommissioned concrete. The IAEA document RS-G-1.7 Application of the Concepts of Exclusion, Exemption, and Clearance, specifies clearance levels of radionuclides' specific activities: a specific activity lower than 0.1 Bq/g for ^{60}Co, ^{152}Eu, and ^{154}Eu allows for a concrete to be recycled after decommissioning of the NPPs. Therefore, low-flux NAA is used to test the detection limits of trace elements in samples

---

[1] Steven Burnham, Greg Moffitt, Quentin Faure, and Tatjana Jevremovic, "Uncertainties in Measuring Trace Amounts of Cobalt and Europium with Low-Flux Neutron Activation Analysis", *Nuclear Technology and Radiation Protection*, Vol. 32, no. 1, 2017. Reprinted with permission.

of cement, coarse, and fine concrete aggregates. These samples are irradiated at the University of Utah's 100 kW TRIGA Reactor (UUTR) at power levels of 10 kW, 30 kW, and 90 kW with the corresponding thermal neutron flux values of $1.5x10^8$, $7.3x10^9$, and $3.76x10^{11}$ neutrons/cm^{2}s. The samples are irradiated for time periods of 1, 3, 30, 60, and 120 minutes. Different power levels and different irradiation times are used to find if there is a threshold set of the NAA parameters in detecting trace amounts of these isotopes. Each of the samples is counted on a Canberra BEGe High Purity Germanium detector. Cement samples are concurrently irradiated with a National Institute of Standards and Technology (NIST) coal fly ash standard reference material and coarse and fine aggregates with Montana soil standard reference material to accurately quantify the mass concentration of the isotopes in concrete samples. The final results show that the reactor power, irradiation, and detector measurement times are heavily correlated in finding the optimum combination for low-flux NAA approach in detecting trace contents of elements, specifically cobalt and europium.

4.2 Introduction

NAA is a nondestructive testing method developed following a discovery of a neutron in 1932, and to date is used to determine elemental composition of an unknown material. A material sample is irradiated with neutrons of preferably thermal range energies, and some of the elements present are activated through neutron capture interactions. Newly created isotopes are radioactive with different decaying times, and energies of the emitted gamma rays are used for identification of (parent) isotopes present in a material sample [47]. Different modes of radioactive decay such as beta emission, positron emission, and isometric transition are often accompanied by gamma rays. The energies of the emitted gamma rays are therefore the signatures uniquely attributed to isotopes by measuring their energies with gamma detectors. The process of NAA is well described in literature [47].

There are different neutron sources used for NAA including: spontaneous fission neutron sources, D-D or D-T generators, and most commonly research reactors. The neutron fluxes therefore vary widely, which holds also for various research reactors as they are directly dependent on both power and reactor core configuration. A comparison of neutron fluxes for some of the research reactors is shown in Fig. 4.2. For example, the Massachusetts Institute of Technology research reactor has a neutron flux on the order of 10^{14} n/cm^{2}s, while the PULSTAR reactor at North Carolina State University has a lower neutron flux on the order of 10^{13} n/cm^{2}s. Similar neutron flux of the same order of magnitude is found in Japan's JRR-4 research reactor [48]. Smaller research reactors such as the University of Utah's 100kW TRIGA Reactor (UUTR) has a neutron flux in a designated thermal NAA port of only $3.76x10^{11}$ n/cm^{2}s. Other low-flux neutrons sources may be used such as ^{252}Cf

whose neutron flux can be on the order of 10^7 n/cm^{2}s [49].The two order of magnitude difference in neutron flux between the UUTR and JRR-4, for example, presents challenges when detecting trace quantities. Elements such as sodium are much easier to detect with a low-flux neutron source due to its high natural abundance. Europium, by contrast, exists in trace quantities and despite having a cross section that is greater, necessitates therefore longer irradiation times in a low neutron flux facility.

Due to recent growing interest in improving concrete in structures of NPPs, we select the concrete aggregates to study the applicability of low-flux NAA in detecting trace quantities of elements. For this study to have applicability in nuclear field, we selected to analyze concrete mixtures for key elements that classify concrete as low-level waste. Concrete is one of the most complex materials used in industry and as such presents the most challenging mixture to analyze for trace quantities of metals. There is a tendency in defining different concrete mixtures assuring its exposure to neutron radiation in NPPs will not activate the mixture above the IAEA limits. The IAEA has defined in its document RS-G-1.7 Application of the Concepts of Exclusion, Exemption, and Clearance, specific limits for disposal of artificially created radionuclides. When a radionuclide is activated at or above the specified limit, that material wherein it is contained must be disposed of as Low-Level Waste (LLW). Factors affecting whether a material will be classified as LLW include total neutron fluence exposed to and the concentration of the radionuclides parent isotope. If an isotope is of sufficiently low concentration, exposure to high neutron fluence may not necessitate disposal as LLW.

The classification of a material as LLW is based on comparing its specified clearance level from IAEA document RS-G-1.7 to its measured activity using the following equation:

$$\sum_{i=1}^{n} \frac{C_i}{CL} \leq 1 \tag{4.1}$$

where C_i is concentration of the artificial radionuclide, (Bq/g), and CL is the IAEA clearance level for artificial radionuclide, (Bq/g). If Eq. 4.1 results in a value less than or equal to one, then that material is classified as normal waste; if above one, the material is considered radioactive waste.

In this paper, we present a methodology of how to analyze low-flux NAA in testing complex concrete mixtures for trace quantities of particular elements. A presented methodology of how to detect the trace carriers for concrete activation is developed together with established thresholds in the measurements of samples using low-flux NAA. Typically, structural concrete of NPPs contains metals and rare earth elements. Specifically, the presence of three nuclides ^{59}Co, ^{151}Eu, and ^{153}Eu, almost always results in the classification of concrete as low-level radioactive waste because their neutron heavier radioisotopes ^{60}Co, ^{154}Eu, and ^{152}Eu, respectively (with half-lives of 5.27, 8.59, and 13.54 years), accumulate the activities above the level of regular (recyclable) waste. The clearance

levels for all three isotopes is 0.1 Bq/g [50]. Their activation is a result of exposure to neutron radiation in nuclear power plants for a period of 40 years or longer. Due to their long decay times, it takes several decades to decay below the clearance levels, accounting for almost 99% of the residual radioactivity in NPPs' concrete shielding walls, [51]. The elimination of these target radionuclides from concrete aggregates has never been considered in the U.S. nuclear power plant design technology. We have started this research with two goals: firstly to define the methodology that is accurate and proven, yet applicable to detection of trace quantities in general, and then to apply this methodology to develop new concrete chemical mixtures resistant to radiation levels above the clearance levels [5].

4.3 Low-Flux NAA Methodology for Identification of Trace Quantities in Solid Samples

4.3.1 Low-Flux NAA at the University of Utah Nuclear Engineering Facility

At the Nuclear Engineering Program at the University of Utah, we manage and operate a 100 kW TRIGA Mark I reactor (UUTR). The reactor and the state-of-the-art radiation counting instrumentations are used in support of education, training, and research. The UUTR is well analyzed and a number of papers report on its flux evaluation and measurements, [52, 53, 54].

NAA is a well-established [47] and commonly used technique at the UUTR facility [55]. The UUTR is equipped with four different irradiation ports: Thermal Irradiator (TI), Fast Neutron Irradiation Facility (FNIF), Pneumatic Irradiator (PI), and a Central Irradiator (CI). All NAA samples are irradiated in the TI or PI. Experimental discrimination between thermal and fast neutrons in the TI is obtained by measuring the cadmium ratio. The cadmium ratio is defined as the ratio of the activity of a bare, gold foil to the activity of a cadmium covered gold foil. The cadmium covered gold foil is activated with mostly fast neutrons because nearly all neutrons below the cadmium cut off energy of 0.4-0.6 eV are absorbed by the cadmium foil. The cadmium ratio in the UUTR TI port is determined to be 4.14 ± 0.015, meaning there is still a high number of fast neutrons in the TI port [54]. A detailed MCNP6 model of the UUTR is always used to determine the flux profile in the reactor core as well as the neutron flux in the irradiation ports of the reactor. The neutron flux distribution as a function of neutron energy inside of the CI, TI, and FNIF at 90 kWth is shown in Fig. 4.1. Knowing the flux profile allows for determining the activities of isotopes activated during irradiation of samples. The TI of the UUTR at a power of 90 kWth has a maximum thermal neutron flux of 3.76×10^{11} neutrons/cm^{2}s. For example, as shown in Fig. 4.2, in the JRR-4 of the Japan Atomic Energy Research Institute, the maximum thermal neutron flux is 7×10^{13} neutrons/cm^{2}s [48]. When using low-flux NAA, it is mandatory to develop a methodology to detected trace quantities

of particular elements and analyze which of the parameters are the most influential in achieving the most accurate measurements: power level, irradiation time, counting time, sample size, and others.

4.3.2 Correlation Between Reactor Power (Neutron Flux), Irradiation/Cooling Time, and Detection Limits in Detecting Trace Quantities: An Example of ^{60}Co, ^{152}Eu, and ^{154}Eu

In order to determine the NAA conditional parameters for detection of trace elements, three reactor power levels (neutron flux) were selected: 10 kW and 30 kW, with a thermal neutron flux of $1.5x10^8$ and $7.3x10^9$ neutrons/cm^{2}s, respectively, are selected to test if this would result in minimal activation to detect trace amounts of Co and Eu; and additionally, 90 kW with thermal neutron flux of $3.76x10^{11}$neutrons/cm^{2}s that still represents an overall low power level compared to other research reactors (as shown in Fig. 4.2). In addition to irradiation time, cooling time of samples (after irradiation in the reactor) is also a variable parameter that requires optimization. Elements with short half-lives such as Na may activate to a sufficiently high level to interfere in the detection of other trace elements requiring longer irradiation times. Finally, counting time is also required to be optimized. A short counting time is preferred as samples can be analyzed more efficiently. However, trace elements may necessitate longer counting times.

Three white cement, quartzite coarse aggregate, and silica sand fine aggregate are selected based on their wide availability. Five samples with a mass of approximately 1g are irradiated for 1, 3, 30, 60, and 120 minutes and at three different power levels using the following method:

- Cement is a finely ground homogenous mixture. Approximately 1g of cement is collected and sealed in a polyvinyl bag for each irradiation time. Five samples are irradiated at each power level totaling 15 cement samples.
- Aggregate samples have a larger particle size and are very heterogeneous. Coarse aggregate is therefore nicely crushed to a fine particle size using a pestle and mortar. The crushed sample is then mixed to create a semi-homogenous sample from which smaller 1g samples are created. Five 1g samples are sealed in polyvinyl bags for irradiation at each power level, thus totaling 15 samples. This same process is used for the fine aggregate samples. Irradiated alongside each cement sample is NIST.
- Irradiated alongside each cement sample is NIST standard reference material 1633c coal fly ash and 2710a Montana soil with each coarse and fine aggregate sample [56, 57].

After irradiation, all samples but cement-based ones are kept for 1-2 weeks before counting on gamma spectroscopy equipment. Cement samples are kept for 24 weeks before counting to reduce a dead time on the detector as well as to reduce interfering signals of short-lived isotopes with high intensity gamma rays such as ^{24}Na and ^{56}Mn. The samples are counted for three (3) hours in point

source geometry by raising them 24 cm off the face of the detector. The reason for raising the samples 24 cm off the face of the detector is due to the high activity of these samples with only a few weeks' time for the short-lived radionuclides to decay away. The high activity of the samples creates as much as 50% dead time on the detector. The dead time can be significantly reduced to less than 1% by raising the sample off the face of the detector (using a spacer). The use of a spacer, however, has the negative effect of reducing the intrinsic efficiency of the detector (number of pulses recorded divided by the number of gamma rays incident on the detector) [58]. As the samples are allowed more time for short-lived radionuclides to decay away, they can eventually be moved directly onto the face of the detector without creating dead time and increase the intrinsic efficiency. In each sample measurement, the activities of all three isotopes are too low to be detected in the aforementioned geometry. A minimum detectable activity (MDA) analysis is therefore applied to each of the counts. The average MDAs for each of the three isotopes is summarized in Table 4.1 and is calculated using the Canberra Genie-2000 software which utilizes the methods developed by Currie [59]. This software calculates the MDA for each gamma-ray of an isotope and uses the smallest calculated value. For example, ^{60}Co has two gamma-rays with an intensity greater than 99%. Genie-2000 would calculate the MDA for each gamma-ray and then assign the smallest value calculated as the MDA for ^{60}Co. The following equation is used to calculate the MDA for each of the radionuclides [60]:

$$MDA = \frac{L_D}{T_1 \epsilon' y V K_c K_w K_x C_f U_f} \tag{4.2}$$

where

L_D = detection limit in counts

T_1 = collection live time in seconds

ϵ' = attenuation corrected efficiency

y = the branching ratio of gamma energy under consideration

V = mass or volume of sample

K_c = correction factor for the nuclide decay counting

K_w = correction factor for the nuclide decay from the time the sample was obtained to collection time

K_x = is an optional correction factor for air samples or irradiated samples and 1 for all other samples

C_f = sample mass conversion factor to translate calculated activity values to the original sample mass

U_f = unit converstion factor from Bq to desired activity units

One of the factors affecting the MDA is the counting time (T_1). With three (3) hours of counting time per each of the samples, the MDA can easily be decreased by increasing the counting time to

12 or 24 hours. Here is one example:

Demonstrating how MDA can be improved, by illustrating how to calculate the MDA for the 569 keV peak of ^{134}Cs for 1.1 hour of counting time using Eq. 4.2 [60]:

$MDA = \frac{406.9}{4000 \times 2.035x10^{-3} \times 0.154 \times 1 \times 0.999 \times 0.934 \times 1 \times 37000} = 9.36 \times 10^{-3} \mu\text{Ci}/\text{g}$

If, for example, the counting time is increased from 4,000 seconds (1.1 hours) to 86,400 seconds (24 hours), the MDA is decreased by one order of magnitude as follows:

$MDA = \frac{406.9}{864000 \times 2.035x10^{-3} \times 0.154 \times 1 \times 0.999 \times 0.934 \times 1 \times 37000} = 4.34 \times 10^{-4} \mu\text{Ci}/\text{g}$

It is therefore shown that increasing the counting time from 1.1 hours to 24 hours decreases the MDA by one order of magnitude.

4.4 Anlysis of the Elemental Mass Concentrations

To determine the mass concentration, the sample of unknown concentration is compared to a Standard Reference Material (SRM). The unknown sample can be compared directly to a known sample with known concentrations of the isotopes of interest using the following correlation:

$$\frac{A_{unk}}{A_{std}} = \frac{m_{unk}}{m_{std}} \frac{\left(e^{-\lambda t_d}\right)_{unk}}{\left(e^{-\lambda t_d}\right)_{std}} \tag{4.3}$$

where

A_{unk} = activity of isotope interest in the unknown sample

A_{std} = activity of isotope of interest in the standard

m_{unk} = mass of isotope interest in the unknown sample

m_{std} = mass of isotope of interest in the standard

t_d =decay time from the end of irradiation to the start of counting

The certified mass concentration values for each SRM used are given in Table 4.2.

As previously shown, the MDA of an isotope can be improved by increasing the counting time. The intrinsic efficiency or number of detected counts divided by the number of gamma-rays incident on the detector can also be improved by moving the sample closer to the face of the detector. An improvement of the intrinsic efficiency and MDA allows for detection of isotopes in trace quantities with low activity.

The samples of cement, fine, and coarse aggregate irradiated for 120 minutes at 10 kW, 30 kW, and 90 kW are further studied since they would have the highest activities of any of the other samples. This is because the samples are exposed to the highest neutron fluence (120 minutes). To improve the MDA, the samples are each counted for 24 hours while intrinsic efficiency is improved by placing samples directly on the face of the detector along with their respective standard reference materials.

In each instance, the activity of the samples is measured to be above the calculated MDA of the Co and Eu isotopes. This allows for a direct calculation of the Co and Eu activities in the samples using Eq. 4.3, the results of which are summarized in Fig. 4.3 and Table 4.3. In each instance, the concentrations were calculated to fall within IAEA established clearance levels. The largest uncertainty occurs in coarse aggregate samples irradiated at 10 and 30 kW and the fine aggregate irradiated at 120 kW. The larger uncertainty in these samples is a result of the low neutron flux. This results in a lower activity to measure and therefore greater uncertainty. The uncertainty is obtained to be 3 sigma or 99.7% confidence interval. It is calculated using the error propagation formula as follows:

$$\sigma = C \times \sqrt{\left(\frac{\sigma_s}{S}\right)^2 \times \left(\frac{\sigma_v}{V}\right)^2 \times \left(\frac{\sigma_{\epsilon'}}{\epsilon'}\right)^2} \tag{4.4}$$

where

$\sigma_c =$ uncertainty of the activity

$C =$ measured activity

$\sigma_s =$ uncertainty in the peak area

$S =$ peak area

$\sigma_v =$ uncertainty in the sample quantity

$V =$ sample quantity

$\sigma_{\epsilon'} =$ uncertainty in the efficiency

$\epsilon' =$ efficiency

The sample quantity and uncertainty are a result of the balance used to measure the mass. The activity and efficiency uncertainty are determined from the detectors calibration. In every instance, the uncertainty of the samples still falls below IAEA clearance levels. The cement samples have the smallest standard deviation in their calculated mass concentrations of each of the three samples. The standard deviation is separate from the mass uncertainty and is used only to compare the calculated mass concentration between the same materials to determine sameness. The standard deviations are: 0.018 and 0.0025 for the Co and Eu, respectively. The standard deviations for the coarse aggregate are 0.067 and 0.0092 for Co and Eu, respectively. The standard deviations for the fine aggregate are 0.079 and 0.011 for Co and Eu, respectively. The standard deviations are larger for the aggregates compared to the cement because of the more heterogeneous nature of the aggregates. While steps were taken to ensure a more homogenous mixture of coarse and fine aggregates, a much larger sample size would be required to decrease the standard deviation between the samples.

These experiments indicate that an optimal set of parameters is to irradiate for 120 minutes at a power level of 90 kW. Although the Co and Eu are detected at the lower power levels, the

uncertainties are larger than when irradiated at a higher power level. Additionally, the samples almost must be counted for 24 hours and directly on the face of the detector to maximize intrinsic efficiency.

4.5 Conclusion

Neutron activation analysis is a common and well-established tool for identification and quantification of elements in trace quantities. Several types of neutron sources can be used to perform NAA including spontaneous fission sources, neutron generators, and research reactors. Since the UUTR is a low-power low-flux research reactor it is required to establish a methodology when quantifying the trace quantities of certain elements. Specific elements of interest are cobalt and europium present in raw concrete materials. The reason why we have selected concrete as a material to test the low-flux NAA at our facility is a very recent growing interest in improving the quality and characteristics of concrete in NPPs. Structural concrete is used as a biological shield in NPP and as such, becomes radioactive due to exposure to neutrons. The IAEA standards outlined in the document RS-G-1.7 define the specific activities of artificially created radionuclides that allow for a material to be disposed of as normal waste or classified as radioactive waste. The defined specific activities are known as an isotopes clearance level and are defined at 0.1 Bq/g for ^{60}Co, ^{152}Eu, and ^{154}Eu, daughter products for naturally occurring Co and Eu. These three isotopes account for over 99% of the residual radioactivity in NPP decommissioned concrete and therefore present a critical element to determine their presence in trace quantities in a given sample. Low-flux NAA at the UUTR is therefore optimized for the detection of these trace elements. The samples of cement, coarse, and fine aggregate are irradiated at three different power levels (of 10 kW, 30 kW, and 90 kW with corresponding neutron flux values of 1.5×10^8, 7.3×10^9, and 3.76×10^{11} neutrons/cm^{2}s, respectively) to understand the lowest power level required when combined with the duration of exposure for a period of 1, 3, 30, 60, and 120 minutes at each power level. The different power levels and irradiation times provided a threshold set of NAA parameters where trace elements of an isotope may be detected with acceptable uncertainties. An exact threshold or minimum value for reactor power level is not strictly recommended as Co and Eu were detected in each instance. However, at the lower power levels, the largest uncertainty in measuring the trace quantities suggest that in case of the UUTR, recommended power level is to be 90 kW. Additionally, the experiments point at 120 minutes of irradiation time and 24 hours of counting as the best combination in detecting trace quantities of Co and Eu with low uncertainty. It is important that all samples are concurrently irradiated alongside a NIST standard reference material in order to calculate the mass concentrations of Co and Eu. Coal Fly Ash was used with cement samples and Montana Soil is used with coarse

and fine aggregate samples.

4.6 Acknowledgement

This research was partially supported by the Utah Nuclear Engineering Program, and partially by the US NRC fellowship program. The initial work was supported by the grant from the American Concrete Institute.

The authors want to thank Jason Rapich for initiating this research while working on his MS degree at the Utah Nuclear Engineering Program. We remain thankful for his continuous support and help in providing us with the concrete aggregate samples.

Authors would like to thank Roy Dunker of Idaho State University for his help on the detection instrumentation.

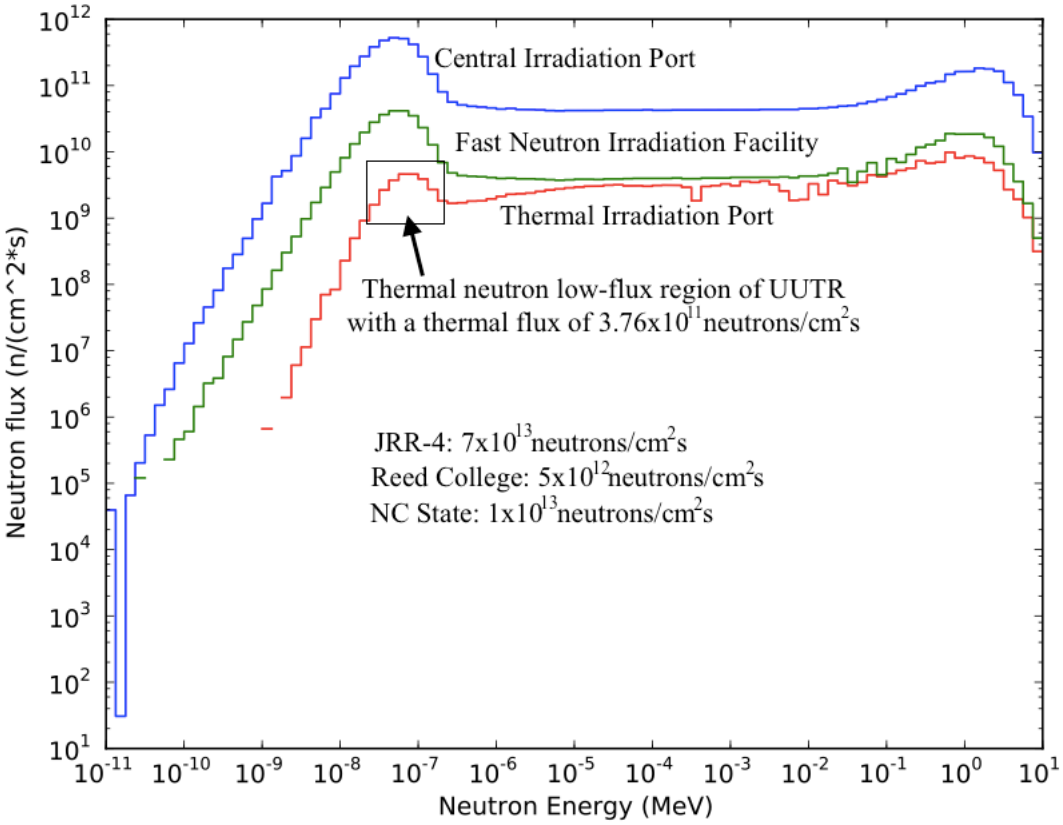

Fig. 4.1: Neutron flux profile as a function of neutron energy in the UUTR irradiation ports (calculated with MCNP6). The UUTR has a maximum thermal neutron flux of 3.76×10^{11} neutrons/cm^{2}s as shown in Fig. 4.2.

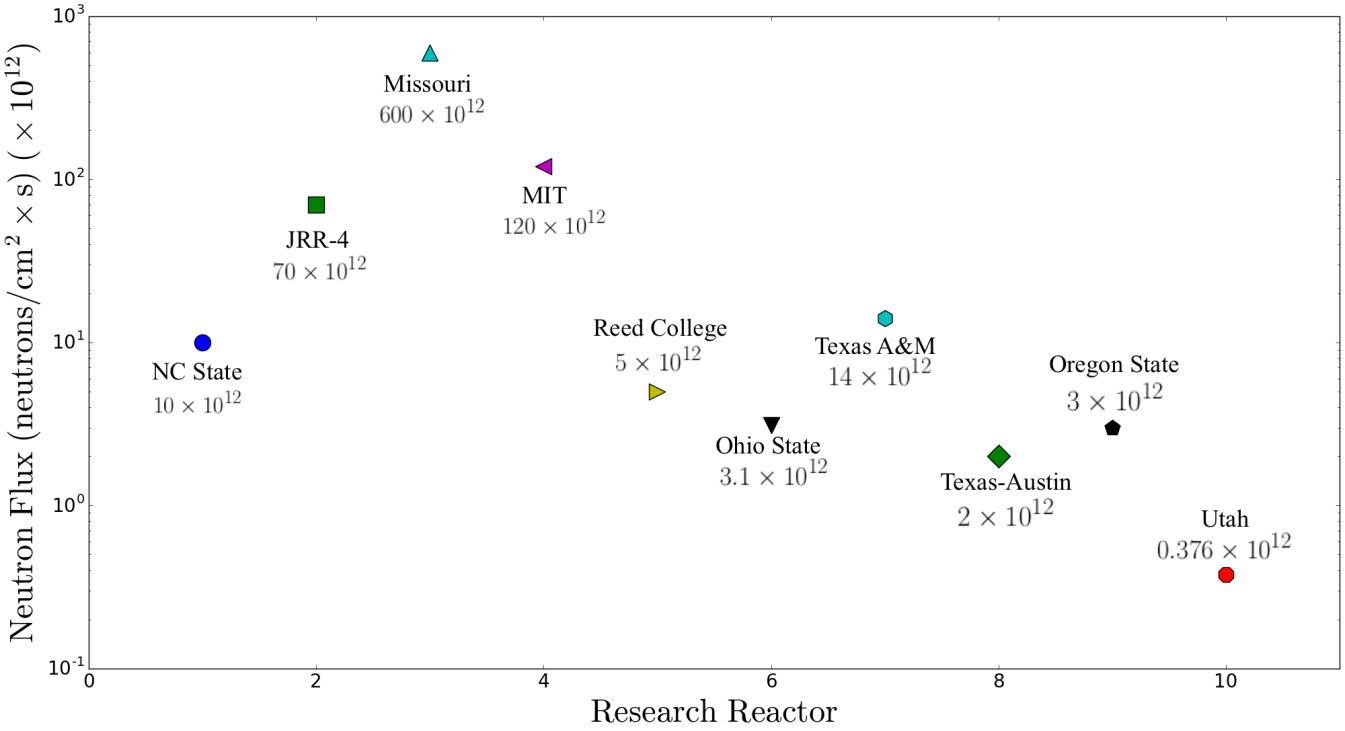

Fig. 4.2: Thermal neutron flux (neutrons/cm^{2}s) for irradiation ports in research reactors with NAA facilities. [Neutron flux data taken from the individual organizations' websites.]

Table 4.1: Average MDA for ^{60}Co, ^{152}Eu, and ^{154}Eu for 3 hours of counting in point source geometry

Isotope	MDA in unknown sample (μCi/g)	MDA in standard reference material (μCi/g)
^{60}Co	$2.0x10^{-4}$	$2.3x10^{-4}$
^{152}Eu	$4.0x10^{-4}$	$4.2x10^{-4}$
^{154}Eu	$3.4x10^{-4}$	$3.6x10^{-4}$

Table 4.2: Certified mass concentrations of Co and Eu in each NIST standard reference material

	1633c Coal Fly Ash	2710a Montana Soil
Element	Mass Concentration (ppm)	Mass Concentration (ppm)
Cobalt	42.9 ± 3.5	5.99 ± 0.14
Europium	4.67 ± 3.5	0.82 ± 0.01

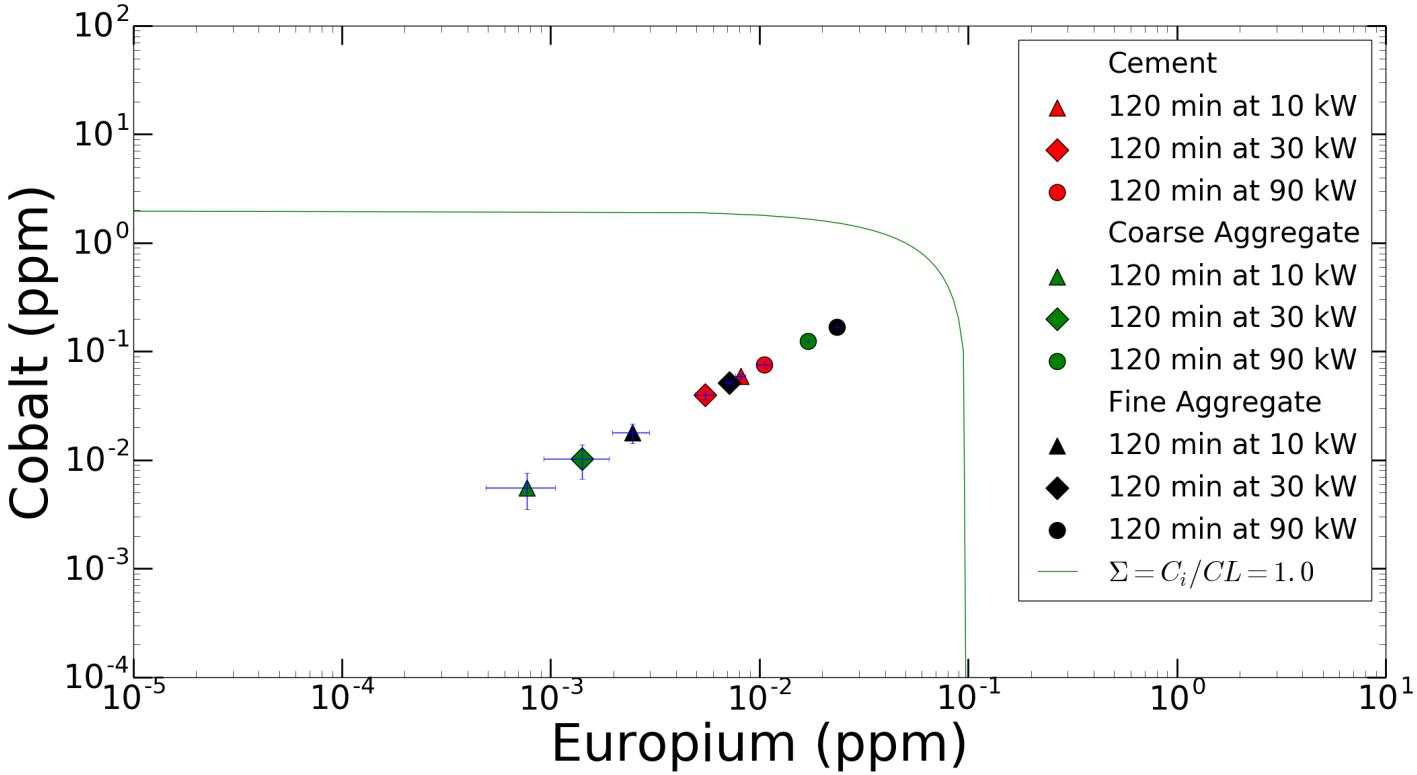

Fig. 4.3: Calculated trace concentrations of Co and Eu in white cement, coarse, and fine aggregates using standard reference material 1333c Coal Fly ash for white cement and 2710a Montana Soil for coarse and fine aggregates. Samples enclosed in the green represent samples that fall below the IAEA established clearance levels for LLW.

Table 4.3: Summary of calculated trace concentrations of Co and Eu in white cement, coarse, and fine aggregates (Fig. 4.3)

Material	Power Level (kW)	Co (ppm)	Eu (ppm)
Cement	10	0.008	0.059
Coarse Aggregate	10	0.001	0.006
Fine Aggregate	10	0.002	0.018
Cement	30	0.005	0.040
Coarse Aggregate	30	0.001	0.010
Fine Aggregate	30	0.007	0.124
Cement	90	0.011	0.076
Coarse Aggregate	90	0.017	0.124
Fine Aggregate	90	0.023	0.169

CHAPTER 5

CONCLUSION AND FUTURE WORK

5.1 Conclusion

Concrete has widespread use within the nuclear industry and serves many purposes such as shielding, physical security, containment, and infrastructure support. Nuclear power plants were originally built with a 30-40-year design lifetime yet economics have now dictated that power plants have a service life of 60-80 years, presenting unique challenges to concrete used in nuclear infrastructure. Little can be done to improve existing concrete structures because 50% or more of ageing concrete problems are related to deficiencies at the time of placement. The most influential time affecting concrete longevity is the curing phase or the first 28 days following its placement. An atomistic-based analysis of concrete chemistry was presented to improve concrete structural properties and longevity.

Concrete chemistry changes that occur when exposed to low-dose gamma radiation during the early curing stage, the first 28-days following mixing, have been shown in improve compressive strength. When gamma rays interact with freshly mixed concrete, a substantial amount of free water to interact with is available. Through the process of radiolysis, free radicals such as H^+ and OH^- are created that may be beneficial to improving compressive strength by improving reactivity between alite, belite, and C-S-H with water and aggregate.

The effects that low-dose gamma radiation has on compressive strength of concrete were studied by exposing concrete cubes to a 630 MBq ^{137}Cs source. The dose to the concrete cubes from the ^{137}Cs source was determined experimentally to be 0.76 Gy for seven days of exposure and calculated using MCNP6 to be 0.66 Gy for seven days of exposure. The compressive strength of gamma cured concrete cubes after seven days showed an increase in compressive strength of 24% with seven days of exposure. After 14 days of exposure the gamma cured cubes had an average compressive strength of 76%, while the 28-days concrete cubes showed no difference in compressive strength.

The microstructure of concrete cubes after seven, 14, and 28 days was analyzed using a Scanning Electron Microscope (SEM). The gamma cured and conventionally cured cubes were found to have

similar microstructure. The similarities in the microstructure from the two different curing methods shows that low-dose gamma radiation does not compromise the integrity of the concrete.

Molecular Dynamics (MD) modeling based on the MOPAC package was used to study how gamma radiation exposure during the curing stage improves compressive strength of concrete. Individual molecules present in un-hydrated cement and concrete were modeled, and their Highest Occupied Molecular Orbital (HOMO) and Lowest Unoccupied Molecular Orbital (LUMO) were calculated. These values represent the reactivity between different molecules. The HOMO and LUMO values were calculated with and without free radicals present from gamma irradiation of concrete. It was shown that the reactivity between un-hydrated cement and concrete molecules responsible for strength improves when free radicals are introduced through gamma irradiation. The increase in reactivity between these molecules leads to an increase in overall compressive strength of concrete.

Concrete chemistry was shown to be controlled by atomistic components ensuring strength is not reduced by that activation from long-term exposure to neutron flux is negligible. To control the atomistic components, a methodology was established to detect trace quantities of Co and Eu in concrete materials using low-flux Neutron Activation Analysis (NAA) in the University of Utah TRIGA Reactor (UUTR). It was shown that long irradiation time and high neutron flux is necessary to minimize uncertainty in measuring elemental composition of trace elements. By carefully selecting concrete components that do not contain Co and Eu which activate to high levels after decades of exposure to neutron flux, the end of life for concrete is improved by declassifying it to be low-level radioactive waste. The economics of commissioning nuclear power plants built in the future are directly improved by significantly reducing the quantity of material that must be disposed of as radioactive waste.

5.2 Future Work

Future work includes some key changes to studying gamma cured concrete. While the same mix design was strictly adhered to for all concrete mixtures, differences between batches have been shown to be significant, making it difficult to compare seven, 14, and 28-day compressive strength values to each other. These inconsistencies are most likely a result of changes in the source of fine aggregate used in mixing. Due to limitations in the size of the gamma irradiator, only 12 concrete cubes may be accommodated at one time. Future mixes should be divided into three sections where four cubes are tested at seven days, four at 14 days, and four at 28 days. The same schedule follows for conventionally cured cubes. This method will allow for seven, 14, and 28 days cured cubes to be directly compared to each other to better understand how gamma curing affects the entire curing

period. The ability to directly compare is a result of the aggregate being consistent for all concrete cubes.

Future Molecular Dynamics (MD) modeling should expand on the molecules modeled. Several forms of C-S-H exist with differing reactivity. Future MD modeling can also determine the stress and strain of different molecules when loading is applied. The stress and strain of the molecules could be correlated with improved compressive strength. The simulations can also help determine which forms of C-S-H are strongest with future simulations determining how to optimize the formation of the strongest forms of C-S-H.

Low-activation concrete should also be further studied. The University of Utah TRIGA Reactor (UUTR) has recently repaired its pneumatic irradiation port. This port has lower flux than many larger reactors, but the flux is higher than exists in the thermal irradiator. This port also allows for more efficient transportation in and out of the UUTR. The same experiments conducted in this port could further optimize the process of studying for trace element content in concrete materials.

REFERENCES

[1] International Atomic Energy Agency, "Ageing Management of Concrete Structures in Nuclear Power Plants," pp. 1–372, Jan. 2016.

[2] J. Wall, *Program on Technology Innovation: Concrete Civil Infrastructure in United States Commercial Nuclear Power Plants*. EPRI, 2010.

[3] S. Burnham and T. Jevremovic, "Examining the Effect of Gamma Radiation Exposure in Early Stage of Concrete Curing on Its Strength and Long-Term Durability," in *Proceedings of ICONE*, (Charlotte), pp. 1–7, Mar. 2016.

[4] S. Burnham, T. Jevremovic, Q. Faure, and J. Tuttle, "Novel Approach to Improved Concrete Strength for Enhanced Safety and Durability of the Nuclear Power Plant Operation ," in *Proceedings of TOPSAFE*, (Vienna), European Nuclear Society.

[5] S. Burnham and T. Jevremovic, "Methodology for Detection of Trace Amounts of Cobalt and Europium in Neutron Shielding Structural ConcreteIn," in *Proceedings of ICONE*, (Makuhari, Chiba, Japan), May 2015.

[6] F. F. M. Lea, *Lea's Chemistry of Cement and Concrete*. Butterworth-Heinemann, Jan. 2004.

[7] P. K. Mehta and P. J. M. Monteiro, *Concrete: Microstructure, Properties, and Materials*. McGraw Hill Professional, Nov. 2013.

[8] R. H. Petrucci, F. G. Herring, J. D. Madura, and C. Bissonnette, *General Chemistry Principles and Modern Applications*. Prentice Hall, June 2010.

[9] Portland Cement Association, "Products."

[10] "Duke Energy announces closing of Crystal River nuclear power plant," May 2013.

[11] M. Fischer, "The severe accident mitigation concept and the design measures for core melt retention of the European Pressurized Reactor (EPR)," *Nuclear Engineering and Design*, vol. 230, pp. 169–180, May 2004.

[12] F. Bouteille, G. Azarian, D. Bittermann, J. Brauns, and J. Eyink, "The EPR overall approach for severe accident mitigation," *Nuclear Engineering and Design*, vol. 236, pp. 1464–1470, Aug. 2006.

[13] D. T. Ingersoll, "Status of Physics and Safety Analyses for the Liquid-Salt-Cooled Very High-Temperature Reactor (LS-VHTR)," Dec. 2005.

[14] D.-H. Hahn, Y.-I. Kim, C.-B. Lee, S.-O. Kim, J.-H. Lee, Y.-B. Lee, B.-H. Kim, and H.-Y. Jeong, "CONCEPTUAL DESIGN OF THE SODIUM-COOLED FAST REACTOR KALIMER-600," *Nuclear Engineering and Technology*, vol. 39, no. 3, pp. 193–206, 2007.

[15] L. Cinotti, C. F. Smith, H. Sekimoto, L. Mansani, M. Reale, and J. J. Sienicki, "Lead-cooled system design and challenges in the frame of Generation IV International Forum," *Journal of Nuclear Materials*, vol. 415, pp. 245–253, Aug. 2011.

[16] C. F. Smith, W. G. Halsey, N. W. Brown, J. J. Sienicki, A. Moisseytsev, and D. C. Wade, "SSTAR: The US lead-cooled fast reactor (LFR)," *Journal of Nuclear Materials*, vol. 376, pp. 255–259, June 2008.

[17] M. Holt and A. Andrews, "Nuclear Power Plants: Vulnerability to Terrorist Attack," Aug. 2007.

[18] ACI Committee 349, *Code Requirements for Nuclear Safety-Related Concrete Structures (ACI 349-06) and Commentary*, Aug. 2007.

[19] T. ICHIKAWA and H. KOIZUMI, "Possibility of Radiation-Induced Degradation of Concrete by Alkali-Silica Reaction of Aggregates," *Journal of Nuclear Science and Technology*, vol. 39, pp. 880–884, Aug. 2002.

[20] B. Pomaro, V. A. Salomoni, F. Gramegna, G. Prete, and C. E. Majorana, "Radiation damage evaluation on concrete shielding for nuclear physics experiments," *Annals of Solid and Structural Mechanics*, vol. 2, pp. 123–142, Nov. 2011.

[21] G. L. Edgemon and R. Anantatmula, "Hanford Waste Tnak System Degradation Mechanisms," 1995.

[22] J. Coderre, "Principles of Radiation Interactions," pp. 1–17, July 2004.

[23] S. Le Caër, "Water Radiolysis: Influence of Oxide Surfaces on H2 Production under Ionizing Radiation," *Water*, vol. 3, pp. 235–253, Dec. 2011.

[24] C. J. Hochanadel, "Effects of Cobalt γ-Radiation on Water and Aqueous Solutions," *The Journal of Physical Chemistry*, vol. 56, pp. 587–594, May 1952.

[25] A. M. Neville, *Properties of concrete; 5th ed.* Harlow England: Pearson, 2011.

[26] Portland Cement Association, "Portland Cement, Concrete, and Heat of Hydration," *Concrete Technology Today*, vol. 18, pp. 1–8, July 1997.

[27] M. S. Abrams, "Compressive Strength of Concrete at Temperatures to 1600F," *Special Publication*, vol. 25, pp. 33–58, Jan. 1971.

[28] K. William, Y. Xi, and D. Naus, "A Review of the Effects of Radiation on Microstructure and Properties of Concretes Used in Nuclear Power Plants.," pp. 1–131, Nov. 2013.

[29] M. Boles and Y. Cengel, *Thermodynamics: An Engineering Approach*. McGraw-Hill Education, Jan. 2014.

[30] T. D. Brown and M. Y. Javaid, "The thermal conductivity of fresh concrete," *Matériaux et Construction*, vol. 3, no. 6, pp. 411–416, 1970.

[31] ASTM International, "Making and Curing Concrete Test Specimens in the Laboratory." ASTM International, 2000.

[32] J. T. Goorley, M. R. James, T. E. Booth, J. S. Bull, L. J. Cox, J. W. J. Durkee, J. S. Elson, M. L. Fensin, R. A. I. Forster, J. S. Hendricks, H. G. I. Hughes, R. C. Johns, B. C. Kiedrowski, R. L. Martz, S. G. Mashnik, G. W. McKinney, D. B. Pelowitz, R. E. Prael, J. E. Sweezy, L. S. Waters, T. Wilcox, and A. J. Zukaitis, "Initial MCNP6 Release Overview - MCNP6 version 1.0," tech. rep., Los Alamos National Laboratory (LANL), Los Alamos, NM (United States), June 2013.

[33] Landauer, "InLight Complete Dosimetry System Solution."

[34] Instron, "Industrial Series HVL Models."

[35] ASTM International, "Standard test method for compressive strength of hydraulic cement mortars (Using 2-in. or [50-mm] cube specimens)," 2002.

[36] D. Hou, H. Ma, and Z. Li, "Morphology of calcium silicate hydrate (C-S-H) gel: a molecular dynamic study," *Advances in Cement Research*, vol. 27, pp. 135–146, Mar. 2015.

[37] S. Agostinelli, J. Allison, K. Amako, J. Apostolakis, H. Araujo, P. Arce, M. Asai, D. Axen, S. Banerjee, G. Barrand, F. Behner, L. Bellagamba, J. Boudreau, L. Broglia, A. Brunengo, H. Burkhardt, S. Chauvie, J. Chuma, R. Chytracek, G. Cooperman, G. Cosmo, P. Degtyarenko, A. Dell'Acqua, G. Depaola, D. Dietrich, R. Enami, A. Feliciello, C. Ferguson, H. Fesefeldt, G. Folger, F. Foppiano, A. Forti, S. Garelli, S. Giani, R. Giannitrapani, D. Gibin, J. J. Gómez Cadenas, I. González, G. Gracia Abril, G. Greeniaus, W. Greiner, V. Grichine, A. Grossheim, S. Guatelli, P. Gumplinger, R. Hamatsu, K. Hashimoto, H. Hasui, A. Heikkinen, A. Howard, V. Ivanchenko, A. Johnson, F. W. Jones, J. Kallenbach, N. Kanaya, M. Kawabata, Y. Kawabata, M. Kawaguti, S. Kelner, P. Kent, A. Kimura, T. Kodama, R. Kokoulin, M. Kossov, H. Kurashige, E. Lamanna, T. Lampén, V. Lara, V. Lefebure, F. Lei, M. Liendl, W. Lockman, F. Longo, S. Magni, M. Maire, E. Medernach, K. Minamimoto, P. Mora de Freitas, Y. Morita, K. Murakami, M. Nagamatu, R. Nartallo, P. Nieminen, T. Nishimura, K. Ohtsubo, M. Okamura, S. O'Neale, Y. Oohata, K. Paech, J. Perl, A. Pfeiffer, M. G. Pia, F. Ranjard, A. Rybin, S. Sadilov, E. Di Salvo, G. Santin, T. Sasaki, N. Savvas, Y. Sawada, S. Scherer, S. Sei, V. Sirotenko, D. Smith, N. Starkov, H. Stoecker, J. Sulkimo, M. Takahata, S. Tanaka, E. Tcherniaev, E. Safai Tehrani, M. Tropeano, P. Truscott, H. Uno, L. Urban, P. Urban, M. Verderi, A. Walkden, W. Wander, H. Weber, J. P. Wellisch, T. Wenaus, D. C. Williams, D. Wright, T. Yamada, H. Yoshida, and D. Zschiesche, "Geant4—a simulation toolkit," *Nuclear Instruments and Methods in Physics Research Section A: Accelerators, Spectrometers, Detectors and Associated Equipment*, vol. 506, pp. 250–303, July 2003.

[38] S. Incerti, A. Ivanchenko, M. Karamitros, A. Mantero, P. Moretto, H. N. Tran, B. Mascialino, C. Champion, V. N. Ivanchenko, M. A. Bernal, Z. Francis, C. Villagrasa, G. Baldacchino, P. Guèye, R. Capra, P. Nieminen, and C. Zacharatou, "Comparison of GEANT4 very low energy cross section models with experimental data in water," *Medical Physics*, vol. 37, no. 9, p. 4692, 2010.

[39] M. A. Bernal, M. C. Bordage, J. M. C. Brown, M. Davídková, E. Delage, Z. El Bitar, S. A. Enger, Z. Francis, S. Guatelli, V. N. Ivanchenko, M. Karamitros, I. Kyriakou, L. Maigne, S. Meylan, K. Murakami, S. Okada, H. Payno, Y. Perrot, I. Petrovic, Q. T. Pham, A. Ristic-Fira, T. Sasaki, V. Štěpán, H. N. Tran, C. Villagrasa, and S. Incerti, "Track structure modeling in liquid water: A review of the Geant4-DNA very low energy extension of the Geant4 Monte Carlo simulation toolkit," *Physica Medica*, vol. 31, pp. 861–874, Dec. 2015.

[40] M. G. Hernández, M. A. G. Izquierdo, A. Ibáñez, J. J. Anaya, and L. G. Ullate, "Porosity estimation of concrete by ultrasonic NDE," *Ultrasonics*, vol. 38, pp. 531–533, Mar. 2000.

[41] H. F. W. Taylor, *Cement Chemistry*. Thomas Telford, Jan. 1997.

[42] W. Khaliq and H. A. Khan, "High temperature material properties of calcium aluminate cement concrete," *Construction and Building Materials*, vol. 94, pp. 475–487, Sept. 2015.

[43] K. Fukui, T. Yonezawa, and H. Shingu, "A Molecular Orbital Theory of Reactivity in Aromatic Hydrocarbons," *The Journal of Chemical Physics*, vol. 20, pp. 722–725, Apr. 1952.

[44] K. Fukui and H. Fujimoto, "An MO-theoretical Interpretation of the Nature of Chemical Reactions. I. Partitioning Analysis of the Interaction Energy," *Bulletin of the Chemical Society of Japan*, vol. 41, pp. 1989–1997, Sept. 1968.

[45] J. J. P. Stewart, "MOPAC2016,"

[46] R. T. Downs and M. Hall-Wallace, "The American mineralogist crystal structure database," *American Mineralogist*, vol. 88, pp. 247–250, Jan. 2003.

[47] R. R. Greenberg, P. Bode, and E. A. De Nadai Fernandes, "Neutron activation analysis: A primary method of measurement," *Spectrochimica Acta Part B: Atomic Spectroscopy*, vol. 66, pp. 193–241, Jan. 2011.

[48] M. KINNO, K.-i. KIMURA, and T. NAKAMURA, "Raw Materials for Low-Activation Concrete Neutron Shields," *Journal of Nuclear Science and Technology*, vol. 39, pp. 1275–1280, Dec. 2002.

[49] D. P. DiPrete, S. F. Peterson, and R. A. Sigg, "Low-flux NAA applications at the Savannah River Site," *Journal of Radioanalytical and ...*, 2000.

[50] International Atomic Energy Agency, "Application of the Concepts of Exclusion, Exemption and Clearance," Aug. 2004.

[51] N. Kakinuma, M. Satou, S. Nogami, A. Hasegawa, K. Abe, M. KINNO, K.-i. KIMURA, T. Tanosaki, and R. Yoshino, "Low-Activation Reinforced Concrete Design Methodology (5)," in *SMiRT*, (Toronto), pp. 1–26, Aug. 2007.

[52] A. Cutic, D. Choe, and T. Jevremovic, "Feasibility study of the university of Utah TRIGA reactor power upgrade - Part I: Neutronics-based study in respect to control rod system requirements and design," *Nuclear Technology and Radiation Protection*, vol. 28, no. 2, pp. 109–117, 2013.

[53] P. Babitz, D. Choe, and T. Jevremovic, "Feasibility study of the university of Utah TRIGA reactor power upgrade - part II: Thermohydraulics and heat transfer study in respect to cooling system requirements and design," *Nuclear Technology and Radiation Protection*, vol. 28, no. 4, pp. 352–361, 2013.

[54] B. Noble, D.-O. Choe, and T. Jevremovic, "Experimental and MCNP5 based evaluation of neutron and gamma flux in the irradiation ports of the University of Utah research reactor," *Nuclear Technology and Radiation Protection*, vol. 27, no. 3, pp. 222–228, 2012.

[55] S. Badza and T. Jevremovic, "Neutron activation analysis of Californian and Japanese rice," *Journal of Radioanalytical and Nuclear Chemistry*, vol. 299, pp. 427–431, Oct. 2013.

[56] National Institute of Standards & Technology, "Standard Reference Material 1633c Trace Elements in Coal Fly Ash," July 2011.

[57] National Institute of Standards & Technology, "Standard Reference Material 2710a Montana I Soil," Apr. 2009.

[58] G. Knoll, *Radiation Detection and Measurement (4th ed.)*. Hoboken, NJ: John Wiley, 2010.

[59] L. A. Currie, "Limits for qualitative detection and quantitative determination. Application to radiochemistry," *Analytical Chemistry*, vol. 40, pp. 586–593, Mar. 1968.

[60] C. T. Publications, "Genie 2000 Customization Tools Manual," pp. 1–563, Jan. 2006.